Unravelling the mechanism of NO and NO_2 storage in ceria: The role of defects and Ce-O surface sites

Anastasia Filtschew and Christian Hess*

Eduard-Zintl-Institut für Anorganische und Physikalische Chemie, Technische Universität Darmstadt, Alarich-Weiss-Str. 8, 64287 Darmstadt, Germany

*Corresponding author at: Eduard-Zintl-Institut für Anorganische und Physikalische Chemie, Technische Universität Darmstadt, Alarich-Weiss-Str. 8, 64287 Darmstadt, Germany.
E-mail address: hess@pc.chemie.tu-darmstadt.de

ABSTRACT

Ceria is an important NO_x storage material often used in combination with barium or zirconia. To elucidate the NO and NO_2 storage mechanism in ceria we employed *in situ* Raman spectroscopy coupled with simultaneous FT-IR gas-phase analysis. The Raman spectra reveal new information about the dynamics of the surface and bulk structure of ceria upon NO_x exposure at 30 °C besides the identification of nitrite and nitrate adsorbates. In particular, Raman spectra provide direct evidence of the involvement of Ce-O surface sites so far not accessible by spectroscopic methods. These Ce-O sites play a key role for NO_x storage, as their amount strongly influences the NO_x storage capacity. A reduction of ceria prior to NO_x exposure resulted in a lower NO_x storage capacity, as long as no strong oxidizing agent (e.g. NO_2) was present to form new Ce-O sites. In the case of NO storage at 30 °C, new reaction pathways are postulated that describe the activation of gas-phase oxygen for ionic nitrite transformation and formation of new NO_x adsorption sites. However, it is shown that the activated oxygen species is not a peroxide, as no correlation was found between the peroxides and formed nitrate and nitrite species. Based on our results, a mechanism for NO and NO_2 storage in ceria was formulated.

Keywords

Ceria, NO_x storage mechanism, *in situ* Raman, defects, NO_x adsorber

1. Introduction

To reduce the stress on environment and health, the emission of toxics has to be reduced. In this connection the exhaust emissions of vehicles are of major relevance. A particular challenge is the NO_x emission of diesel engines. Currently, in diesel engines the NO_x is treated by a Selective Catalytic Reduction (SCR) catalyst [1]. However, effective NO_x conversion by the SCR catalyst is only realized at temperatures above 200°C. According to a publication by the Ford Motor Company, the upstream of a SCR catalyst of a 4.4 L diesel engine takes at least 150 s to reach a temperature of 200°C [2]. At

temperatures below 200°C the SCR catalyst converts NO_x with only low efficiency. To improve the NO_x conversion at low temperatures a combination of a Lean NO_x Trap (LNT) and a SCR catalyst could be used [3]. LNTs are often composed of a NO_x storage material, such as ceria or barium, and a precious metal, for instance platinum or palladium, to oxidize NO to NO_2. At low operating temperatures and under lean conditions the NO_x reacts with the LNT, forming predominantly nitrate species. After the LNT is saturated, it has to be regenerated. As the nitrate species are stable, the regeneration has to proceed under rich conditions, so that the stable nitrates decompose to NO_x and can then be converted with suitable reductants to N_2 and O_2 [4, 5]. At temperatures above 200°C, the SCR catalyst becomes active for NO_x treatment. For NO_x treatment by SCR catalysts urea injection is needed. Urea decomposes to carbon dioxide and ammonia, which subsequently reacts with NO_x to give nitrogen and water [6].

However, a regeneration of the NO_x storage material at lean conditions is highly desirable. Therefore, another solution is the combination of a passive NO_x adsorber (PNA) with the SCR catalyst, which was first mentioned by the Ford Motor Company in 2001 [7]. The task of the PNA is to store the NO_x during cold starts and to subsequently release it at temperatures above 200°C under lean conditions, where the SCR catalyst shows high NO_x conversion. Therefore, the PNA is solely a NO_x storage material and does not contribute to the NO_x conversion itself. Furthermore, the PNA should be durable under lean conditions at 800–850°C and completely regenerate at 700–750°C [3].

Common to the LNT and PNA is the NO_x storage in a material at temperatures at which the SCR catalyst is not yet operational. Different NO_x storage materials have been discussed in the literature, such as $Pt/K/Al_2O_3$ [8, 9], $Pt/BaO/Al_2O_3$ [10-12], precious metal promoted Al_2O_3 and La/Al_2O_3 [13], precious metal promoted ceria [3, 11, 14-16], mixtures of Pt/CeO_2 and $Pt/BaO/Al_2O_3$ [11, 17-19], BaO/CeO_2 [20], $Pt/BaO/CeO_2$ [11, 21], and precious metal promoted $Ce_xZr_{1-x}O_2$ [5, 22]. Therefore, ceria is often used in combination with other NO_x storage materials such as barium or zirconia. One benefit of ceria is that it can store NO_x at room temperature [23] and support sulfur resistance [21, 24, 25]. Among ceria-containing PNA materials, Ce-Zr mixed oxides have been considered as interesting candidates for technical applications owing to their oxygen storage capacity mobility as well as their thermal stability [22].

In the literature, different reaction pathways have been discussed for NO_2 (eqs. 1-7) [19, 23, 26-29] and NO storage (eqs. 8-16) [14, 23, 26-28, 30, 31] in ceria. In this context, the ability of ceria to change the oxidation state of cerium and to create oxygen vacancies is crucial for NO_x storage.

$$Ce^{4+}\text{-}O^{2-} + NO_2 \rightarrow Ce^{3+}\text{-}NO_3^- \quad (1)$$

$$2Ce^{4+}\text{-}OH^- + NO_2 \rightarrow Ce^{4+}\text{-}NO_3^- + Ce^{3+}\text{-}\square + H_2O \quad (2)$$

$$Ce^{3+}\text{-}\square + NO_2 \rightarrow Ce^{4+}\text{-}O^{2-} + NO \quad (3)$$

$$Ce^{3+}\text{-}\square + NO_2 \rightarrow Ce^{4+}\text{-}NO_2^- \quad (4)$$

$$Ce^{4+}\text{-}NO_2^- + Ce^{4+}\text{-}O^* \rightarrow Ce^{4+}\text{-}NO_3^- + Ce^{3+}\text{-}\square \quad (5)$$

$$Ce^{4+}\text{-}NO_2^- + NO_2 \rightarrow Ce^{4+}\text{-}NO_3^- + NO \quad (6)$$

$$2Ce^{4+}\text{-}NO_2^- \rightarrow Ce^{4+}\text{-}NO_3^- + Ce^{3+}\text{-}\square + NO \quad (7)$$

$$Ce^{4+}\text{-}O^{2-} + NO \rightarrow Ce^{3+}\text{-}NO_2^- \quad (8)$$

$$2Ce^{4+}\text{-}OH^- + NO \rightarrow Ce^{4+}\text{-}NO_2^- + Ce^{3+}\text{-}\square + H_2O \quad (9)$$

$$Ce^{3+}\text{-}\square + NO \rightarrow Ce^{4+}\text{-}NO^- \quad (10)$$

$$Ce^{3+}\text{-}\square\text{-}Ce^{3+} + NO \rightarrow Ce^{4+}\text{-}NO^{2-}\text{-}\ Ce^{4+} \quad (11)$$

$$Ce^{4+}\text{-}NO^- + Ce^{4+}\text{-}O^* \rightarrow Ce^{4+}\text{-}NO_2^- + Ce^{3+}\text{-}\square \quad (12)$$

$$2\ Ce^{4+}\text{-}NO^- \rightarrow Ce^{4+}\text{-}N_2O_2^{2-}\text{-}\ Ce^{4+} \quad (13)$$

$$Ce^{4+}\text{-}N_2O_2^{2-}\text{-}Ce^{4+} \rightarrow Ce^{4+}\text{-}O^{2-}\text{-}Ce^{4+} + N_2O \quad (14)$$

$$Ce^{3+}\text{-}\square\text{-}Ce^{3+} + N_2O \rightarrow Ce^{4+}\text{-}O^{2-}\text{-}Ce^{4+} + N_2 \quad (15)$$

$$3\ Ce^{3+}\text{-}\square\text{-}Ce^{3+} + Ce^{3+} + 3\ NO \rightarrow 3\ Ce^{4+}\text{-}O^{2-}\text{-}Ce^{4+} + Ce^{4+} + N_3^- \quad (16)$$

In the above equations, O* and □ refer to an activated surface oxygen and a surface oxygen vacancy, respectively. In the literature, the NO_x storage was predominantly investigated for precious metal (e.g. Pt) loaded ceria samples [3, 5, 11, 14-19, 21]. However, to be able to elucidate the role of ceria for NO_x storage in detail, as a first step we have studied the behavior of bare ceria with no other components (e.g., Pt) present. Furthermore, the NO_x storage of ceria was commonly investigated by Diffuse Reflectance Infrared Fourier Transform (DRIFT) spectroscopy [5, 11, 14-17, 32, 33] but rarely by Raman spectroscopy [23, 34]. DRIFT spectroscopy is sensitive to the surface and therefore to adsorbates on the ceria surface. Depending on pretreatment of ceria, temperature and gas composition during NO_x storage, DRIFT spectroscopy detects different surface species. The NO_2 storage in ceria has been shown to result in the formation of predominantly nitrates and some nitrites [14-16, 27, 33, 35]. However, different reaction pathways for the NO_2 storage are discussed. NO_2 can either be stored directly by reaction with surface oxygen (eq. 1) [14, 23, 36, 37] or hydroxide (eq. 2) [26, 27] or can re-oxidize the ceria surface forming NO (eq. 3) [23, 27, 29, 36, 37]. On the other hand, NO in turn can adsorb on the ceria surface forming nitrites according to eqs. 8 and 9 [14, 23, 26, 27, 31, 33]. Nitrites could also arise by direct adsorption of a NO_2 on an oxygen vacancy (eq. 13) [22, 26, 27, 29, 31]. However, nitrites are partially transformed to nitrates, and for such nitrite transformation reaction pathways 5-7 were suggested [14, 19, 26, 27, 31]. Upon NO exposure also the formation of nitrite and nitrate was detected, while in the beginning predominantly nitrite was formed [19, 27, 31, 33, 35]. In literature, the formation of nitrite is discussed to result from the reaction of NO with surface oxygen (eq. 8) [23, 33] or with hydroxide (eq. 9) [14, 26, 27, 31]. However, Mihaylov *et al.* concluded, that upon NO exposure hydroxides are not involved in the nitrite formation [30]. Another possibility to store NO is the absorption of NO on a surface oxygen vacancy, whereas either the formation of a nitrosyl- (NO^-) (eq. 10) [14, 22, 27, 31] or nitric oxide dianion-species (NO^{2-}) (eq. 11) is discussed [30]. The formed NO^- can then be oxidized by an activated surface oxygen (O*) to form nitrite (eq. 12) [14, 27, 31]. Furthermore, Atribak *et al.* and Azambre *et al.* proposed, that NO is initially oxidized to NO_2 and subsequently adsorbs at an oxygen vacancy and forms nitrite (eq. 4) [22, 26, 27, 29, 31]. By contrast, Luo *et al.* discussed the direct storage of NO in ceria without NO_2 formation [16]. Later, a decrease of nitrite and an increase of nitrate was observed and therefore a transformation of nitrite to nitrate was proposed

[15, 19, 27, 31, 33, 35]. For the nitrite transformation again reaction pathways 5-7 were considered [19, 27, 31]. Besides the formation of nitrites and nitrates, also the formation of *cis*- and *trans*-hyponitrites was discussed arising from a dimerization of two nitrosyls (eq. 13) [28, 30, 31, 35]. These hyponitrites can then decompose to N_2O re-oxidizing the ceria surface (eq. 14) [30]. N_2O can in turn readsorb on the ceria surface subsequently decomposing to N_2 (eq. 15) and healing another surface oxygen vacancy [30]. Therefore, in literature, not only NO storage, but also ceria induced NO conversion to N_2 is discussed. In that context, Mihaylov *et al.* also observed the formation of N_3^- (eq. 16), which is a precursor of N_2 [30]. It should be noted that reaction pathways 11 and 14-16 were only observed on reduced ceria upon NO exposure without oxygen and at low pressure [30]. Besides adsorbed NO_x species the $^2F_{5/2} \rightarrow {}^2F_{7/2}$ electronic transition of Ce^{3+} ions can be observed in DRIFT spectroscopy [30, 31]. As discussed by Mihaylov *et al.*, the assignments of NO_x species in DRIFT spectroscopy are controversial [30]. Compared to DRIFT spectroscopy, Raman spectroscopy has the advantage that it monitors not only adsorbates on the ceria surface, but also bulk properties of ceria, for example defects and changes in the lattice constant [38]. Additionally, as our recent studies show, information about surface oxygen on ceria is accessible [39]. Based on this knowledge, we have investigated the NO_2 and NO storage mechanism of ceria by *in situ* Raman spectroscopy coupled with simultaneous FT-IR gas-phase analysis. Our investigations were realized with a fluidized bed approach to avoid sample degradation by laser radiation. Prior to NO_x storage the ceria was treated under either oxidative or reductive conditions, leading to different defect concentrations. Besides the influence of defects the influence of gas-phase oxygen and lattice oxygen was elucidated by performing NO_2 and NO storage experiments on oxidized ceria in the absence of oxygen. The implications of the spectroscopic findings for the NO_2 and NO storage mechanism will be discussed.

2. Experimental Section

2.1 Material Synthesis

The ceria sample was prepared by twofold calcination of cerium(III) nitrate hexahydrate (Sigma Aldrich, 99.999% trace metal basis) at 600°C for 12 h using a heating rate of 6°C/min. After calcination the sample was sieved to achieve particle sizes of 200-300 μm.

2.2 Sample Characterization

The ceria sample was characterized by X-ray diffraction experiments and nitrogen adsorption-desorption measurements. X-ray diffraction experiments were carried out in transmission geometry on a X-ray powder diffractometer (StadiP, Stoe & Cie GmbH) with a Mythen 1K (Dectris) detector. For the measurements a Cu Kα1 radiation (λ= 1.540598 Å) and a Ge[111] monochromator was used. The ceria sample was mixed with a NIST standard (LaB_6, *a*(299 K) = 4.15695 Å, crystal size <10 μm) to correct the positions of the reflections and width of reflections caused by instrumental parameters.

Nitrogen adsorption measurements were carried out on a NOVA 3000e (Quantachrome) to determine the specific surface area. For determination the Brunauer-Emmett-Teller (BET) method was used. Prior to measurements, the ceria was treated in vacuum at 150 °C for 24 h.

2.3 Experimental Setup

The experimental setup is shown schematically in Fig. 1. The investigations were performed with a commercial CCR1000 catalyst cell (Linkam Scientific Instruments). The ceramic sample holder was loaded with 130 mg of the ceria sample on a ceramic fiber fleece and can be heated by a ceramic heating element. While the feed was flowed through the sample from top to bottom, a membrane pump was placed downstream of the catalyst cell to create pressure oscillations. These oscillations then generate a fluidized bed [40].

The Raman spectra were recorded in a backscattering geometry. For excitation, an argon ion laser (514 nm, Melles Griot) and for collection of the backscattered light a transmission spectrometer (Kaiser Optical) equipped with a charge-coupled device (CCD) detector was used. The spectrometer was calibrated using the emission lines of a standard argon lamp. The resolution of the spectrometer was 5 cm^{-1} and the wavelength stability was better than 0.5 cm^{-1}. The laser power was adjusted to 2.3 mW at the location of the sample as measured with a power meter (Ophir). The features in the Raman spectra were fitted by Voigt functions using a Gaussian linewidth of 6 cm^{-1} to describe the instrumental broadening.

The outlet gases were analyzed using a FT-IR spectrometer (Bruker Tensor 27, DLaTGS (deuterated and L-alanine-doped triglycine sulfate) detector), which was equipped with a low volume gas cell (25 mL, 0.5 m pathlength, Axiom, LFT). The gas cell was heated to 125°C to avoid condensation. IR spectra were recorded with a resolution of 4 cm^{-1} and an aperture of 6 mm. For the concentration determination of the gas-phase components calibration curves were recorded. By subtracting the breakthrough curves of the loaded catalyst cell from the empty catalyst cell, the NO_x storage capacity was calculated.

Prior to the NO_x storage experiments the sample was treated to receive either a low defective (oxidative treatment) or more defective ceria (reductive treatment). For the oxidative treatment the sample was heated to 400°C in 20% O_2/N_2 flow for 1 h and cooled afterwards to 30°C using a heating rate of 20°C/min. The more defective ceria was obtained by heating the sample to 400°C in 20% O_2/N_2 for 30 min using a heating rate of 20°C/min. Then the gas flow was switched to pure nitrogen for 5 min to remove the oxygen followed by 30 min of 7.5% H_2/Ar flow. Afterwards the sample was cooled to 30°C in nitrogen using a cooling rate of 20°C/min followed by 10 min of 20% O_2/N_2 flow at 30°C.

NO_x storage with oxygen was performed at 30°C by mixing either 1000 ppm NO_2/N_2 or 1000 ppm NO/N_2 with nitrogen and oxygen to obtain a gas reaction mixture of 500 ppm NO_x/20% O_2/N_2. For the NO_x storage in the absence of oxygen, either 1000 ppm NO_2/N_2 or 1000 ppm NO/N_2 was mixed with nitrogen to obtain a gas reaction mixture of 500 ppm NO_x/N_2. The NO_x storage experiments in the absence of oxygen were performed at 30°C and additionally with NO at 200°C. During NO_x storage and treatment, gas mixtures passed through the catalyst bed at a flow rate of 50 ml min^{-1}, resulting in a gas hourly space velocity (GHSV) of 160000 h^{-1}.

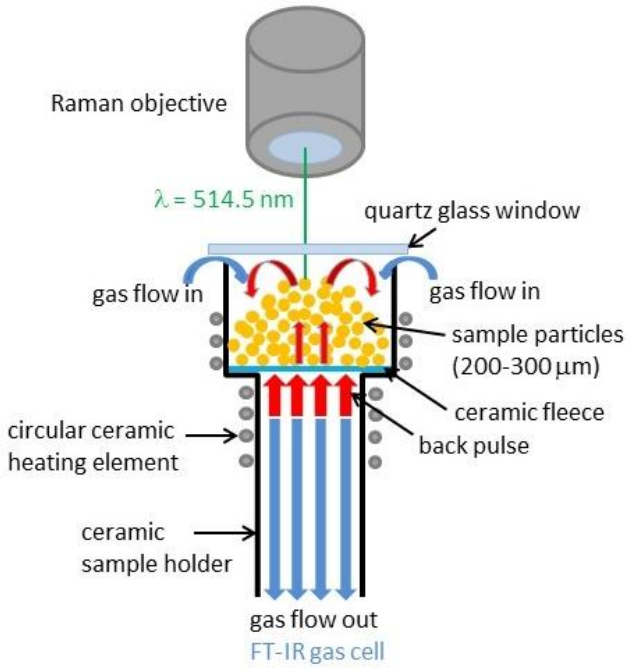

Fig. 1. Schematic drawing of the experimental setup.

3. Results

3.1 Sample characterization

In Table 1, the physical properties of the prepared ceria powder are listed. The X-ray diffraction pattern of the ceria powder contained diffraction lines corresponding to (111), (200), (220), (311), (222), (400), (331), (420) and (422) crystal planes (not shown). The determined lattice parameter of the characteristic fluorite crystal structure of ceria was 5.4121 Å and the average crystal size was estimated as 25-30 nm using Scherrer's equation. From N_2 adsorption-desorption measurements a specific surface area of 64.5 m²/g was calculated, which is similar to the specific surface areas obtained by precipitation methods with subsequent calcination at 500°C [14, 27, 41]. Furthermore, a pore volume of 0.185 cm³/g with an average pore diameter of 139.44 Å was determined.

Table 1

Physical properties of the ceria sample.

	average crystal size (nm)	lattice parameter (Å)	specific surface area (BET) (m²/g)	pore volume (cm³/g)	average pore diameter (Å)
ceria, as prepared	25-30	5.4121	64.5	0.185	139.44

3.2 Pre-treatment

Fig. 2 depicts Raman spectra of ceria after oxidative (red) and reductive (blue) treatment. Spectra were normalized by the F_{2g} mode to account for differences in experimental conditions. The Raman spectra are characterized by features at 250, 407, 464.5, 550, 595, and 1170 cm^{-1}. Recently, Schilling et al. [39] ascribed the features at 250 and 407 cm^{-1} to Ce-O surface vibrations. The dominant feature at 464.5 cm^{-1} originates from a symmetrical stretching of the CeO_8 cubes assigned as the F_{2g} mode [42, 43]. The features at around 550 and 595 cm^{-1} can be attributed to $Ce^{4+}O_7V_O^{\bullet\bullet}$ and $Ce^{3+}O_7V_O^{\bullet\bullet}$ cubes in the ceria lattice, respectively [39]. However, Weber et al. [43] assigned features at 550 and 600 cm^{-1} to second-order Raman features, resulting from mixing of A_{1g}, E_g, and F_{2g} CeO_2 modes. Consequently, bulk features overlap with defect features and cannot be clearly separated. The feature at 1170 cm^{-1} was attributed to a second-order Raman mode assigned as 2LO [43]. For the reductively treated ceria a weak feature at 831 cm^{-1} was observed (see Fig. 2b), which was assigned to the O-O stretching vibration of peroxides [44, 45]. Furthermore, features at 3635 (II-B) and 3650 cm^{-1} (II-A) for the oxidatively and at 3663 (II*-B), 3688.5 (II*-A), and 3714 cm^{-1} (I) for the reductively treated ceria were observed (see Fig. S1), which are assigned to the O-H stretching vibration of hydroxides [46, 47].

Comparison of the differently treated ceria samples revealed significant changes. After reductive treatment, ceria showed lower Ce-O intensities (see Fig. 2a), whereas the intensities of the hydroxides were higher (see Fig. S1). Additionally, the hydroxide features of the reductively treated ceria were blue-shifted. Besides, a weak peroxide feature resulting from oxygen adsorption on two electron defects was observed (see Fig. 2b), which was absent after oxidative treatment [44]. Therefore, the Raman spectra confirm a reduction of the ceria surface after reductive treatment. Moreover, the F_{2g} feature of the reductively treated ceria was redshifted by 0.2 cm^{-1}, hence indicating a slightly larger amount of defects in the lattice. Since the background in the region between 200 and 700 cm^{-1} was lower for the reductively treated ceria, the features at 550 and 595 cm^{-1} probably had a comparable intensity to that for the oxidatively treated ceria.

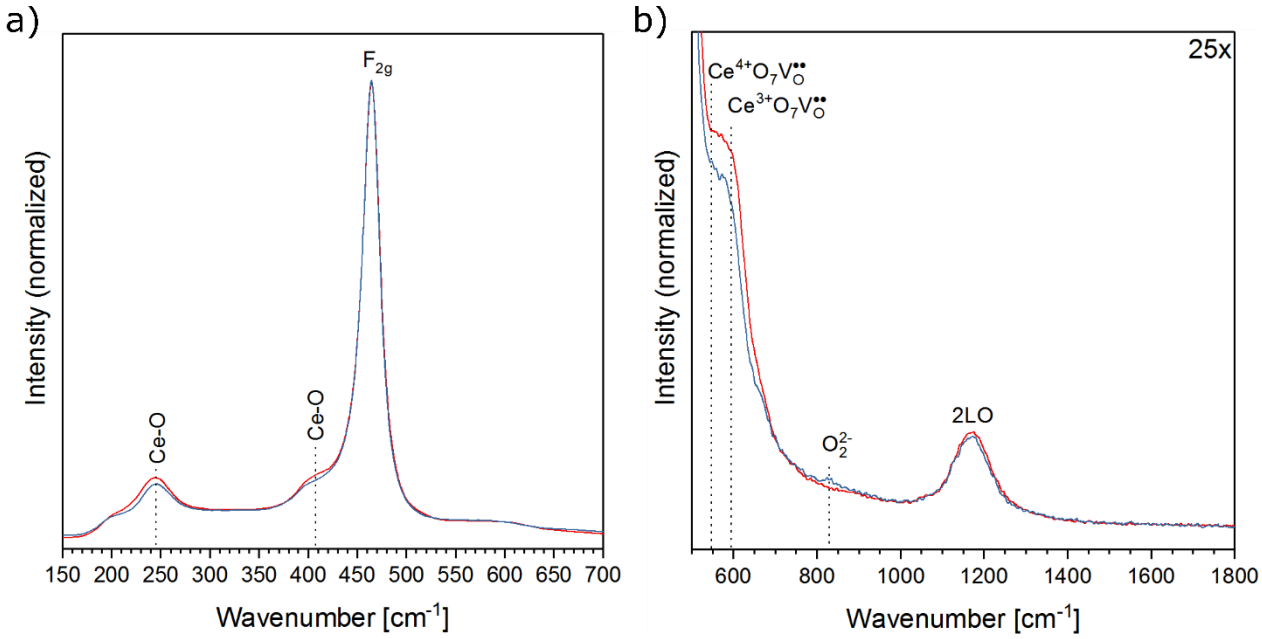

Fig. 2. Raman spectra of ceria recorded at 30°C after oxidative (red) and reductive (blue) treatment showing a) the spectral region 150-700 cm^{-1} b) an enlarged view of the spectral region 500-1800 cm^{-1} (25x magnification). Spectra were normalized by the F_{2g} mode.

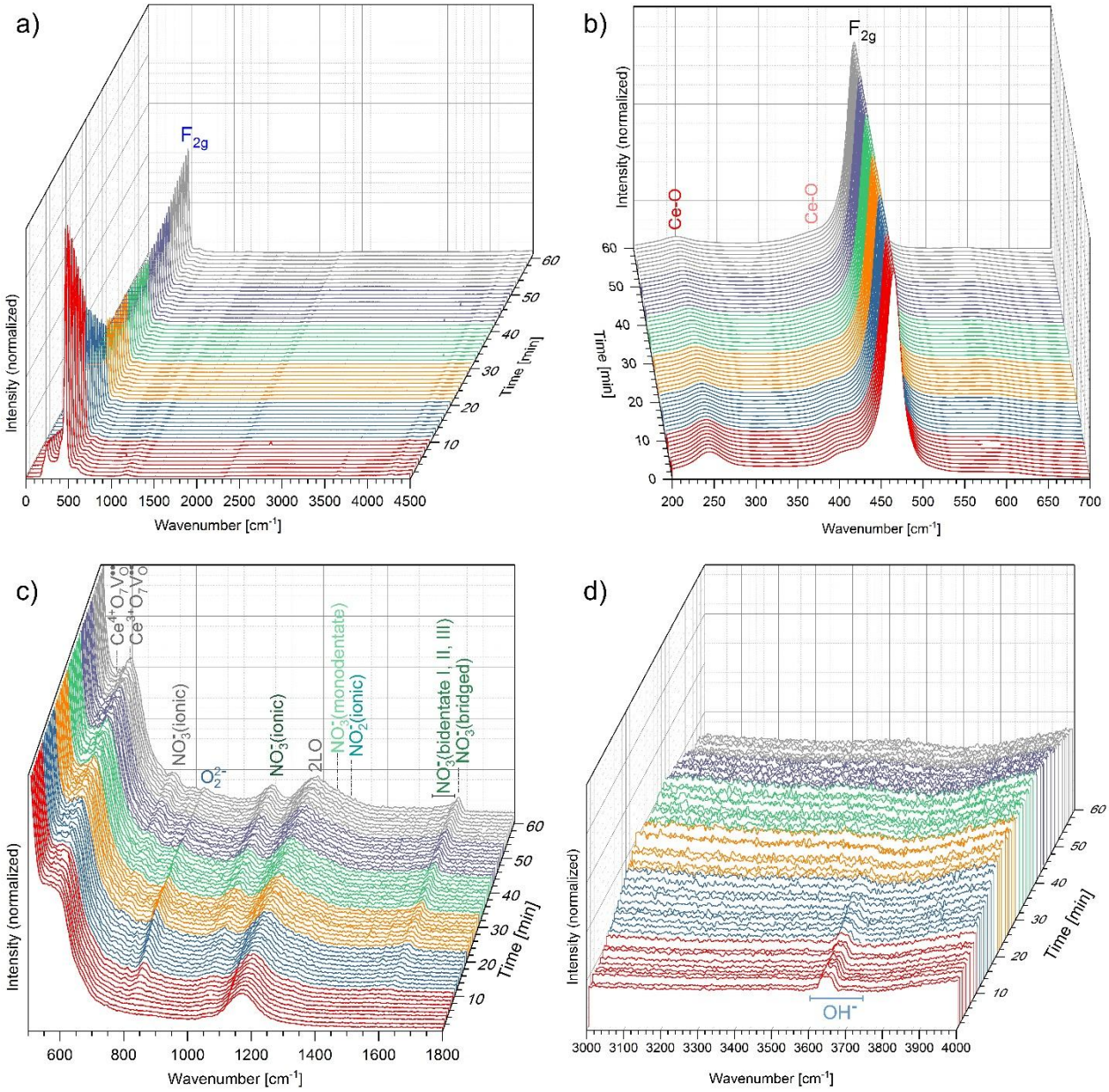

Fig. 3. (a) *In situ* Raman spectra of oxidatively treated ceria showing the temporal evolution upon exposure to 500 ppm NO_2/20% O_2/N_2 at 30°C. An enlarged view of the Raman spectra is shown for the regions (b) 200-700 cm^{-1}, (c) 500-1800 cm^{-1}, and (d) 3000-4000 cm^{-1}.

3.3 NO_2 storage with oxygen at 30°C after oxidative treatment

Fig. 3a displays raw *in situ* Raman spectra of oxidatively treated ceria upon exposure to 500 ppm NO_2/20% O_2/N_2 at 30°C. As could be shown previously, Raman spectra are affected by absorption effects, leading to the intensity dynamics seen in Fig. 3a [48]. As the ceria sample shows changes in the absorption at the laser excitation wavelength at 514 nm, an absorption correction needs to be applied. To obtain the absorption-corrected temporal evolution of the Raman features, the Raman spectra were

normalized by the F_{2g} intensity. Fig. 3b, 3c, and 3d give enlarged views of the absorption-corrected Raman spectra of the regions 200-700 cm^{-1}, 500-1800 cm^{-1}, and 3000-4000 cm^{-1}, respectively.

As a result of NO_2 storage, new Raman features at around 726, 830, 1036, 1248, 1292, 1556, 1584, 1605, and 1622 cm^{-1} emerge during the *in situ* experiment (see Fig. 3c). The features at 726 and 1036 cm^{-1} are assigned to the bending and stretching vibrations of ionic nitrate, respectively [49, 50]. The broad shoulder at higher wavenumbers of the 2LO feature contains two components at 1248 and 1292 cm^{-1} (see Fig. S2). The feature at 1248 cm^{-1} is ascribed to monodentate nitrate [51], whereas the feature at 1292 cm^{-1} is assigned to the symmetrical stretching vibration of ionic nitrite. Due to the low ionic nitrite concentration the symmetrical bending vibration at around 800 cm^{-1} is not observed [52], whereas the feature at 831 cm^{-1} originates from peroxides (see Fig. 3c). The weak features at 1556, 1584, 1605, and 1622 cm^{-1} are attributed to bidentate nitrate III, bidentate nitrate II, bidentate nitrate I, and bridged nitrate, respectively, in agreement with the literature [49]. The different nitrate and nitrite species are illustrated in Fig. 4. Please note that the structures of the ionic nitrite and nitrate are not intended to represent a preferred geometry towards the ceria surface.

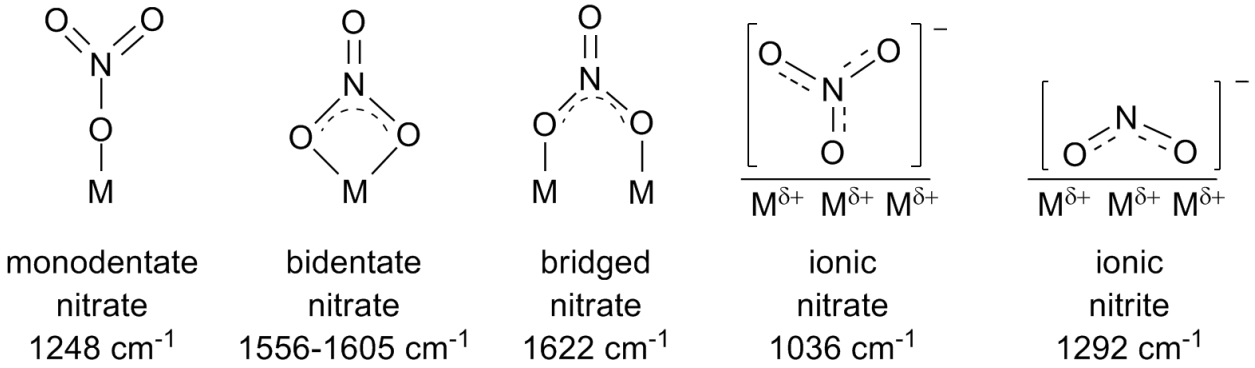

Fig. 4. Illustration of different nitrate and nitrite species with typical wavenumber values observed in this study.

As can be seen in Fig. 3c, upon NO_2 exposure, new Raman features appeared and changes in the characteristic ceria features were observed. The intensity of the peroxide feature at 831 cm^{-1} increased within the first 15 min followed by a subsequent decrease, indicating a dynamical behavior of the surface defects. Additionally, an intensity increase of the Raman feature at 595 cm^{-1} was observed, suggesting an increase in the number of bulk defects (see Fig. 3c), which is confirmed by the redshift of the F_{2g} feature resulting from lattice expansion caused by oxygen vacancies in the bulk (see Fig. 5a). The intensities of the surface oxygen- and hydroxide-related features started to decrease upon NO_2 exposure. After 35 min no more hydroxides could be detected (see Fig. 3d), while surface oxygen was still observable (see Fig. 3b).

To elaborate correlations between characteristic ceria features and emerging nitrate and nitrite species, the areas of the Ce-O, peroxide, hydroxide, ionic nitrate, ionic nitrite, and bidentate/bridged nitrate features, as well as the F_{2g} peak position, were traced (see Fig. 5a-c). For the determination of the nitrate and nitrite areas, the F_{2g}-normalized spectra during NO_2 exposure had the normalized spectra of treated ceria prior to NO_2 exposure subtracted from them. After subtraction the features were fitted by Voigt functions (see Fig. S2). The area of the Ce-O feature at 250 cm^{-1} was also determined from difference spectra, whereas the areas of the peroxide and hydroxide features were determined from normalized spectra. Simultaneously to the Raman spectra, the NO_x concentrations at the outlet were monitored by FT-IR gas phase spectroscopy (see Fig. 5d). As a reference, the dashed line in Fig. 5d indicates the NO_2 inlet concentration. Please note that the type of data presentation introduced in Fig. 5 will also be used to present the results of the other NO_x storage experiments described below.

Since peroxides originate from oxygen adsorption on two electron defects, they provide information on surface defects [44, 39]. The peroxides initially increased as a result of oxygen surface defect creation upon NO_2 exposure (see Fig. 5b), reaching their maximum area after about 15 min followed by a slow decay to nearly zero. In addition to this surface defect dynamics, a F_{2g} redshift of 1.5 cm^{-1} was observed, progressing over the whole 60 min of NO_2 storage. Initially, the F_{2g} feature showed nearly no redshift, then the dynamics became faster and slowed down again after 30 min. As a redshift is caused by formation of oxygen vacancies in the lattice, it predicts a formation of bulk defects in ceria upon NO_2 storage [39]. A similar temporal behavior as for the F_{2g} peak position was also observed for the intensity of the Ce-O feature at 250 cm^{-1} (see Fig. 5b), describing a dependence of bulk defects on surface oxygen consumption. Furthermore, the intensity of the hydroxides decreased to zero within the first 30 min.

During NO_2 storage different types of nitrates and nitrites were formed (see Fig. 5c). Within the first 13 min, the ionic nitrite showed the highest formation rate, reaching its maximum area after 25 min and then decreasing again within the further course of the experiment to a final value of 0.0025. Monodentate nitrate was not observed within the first 8 min, but emerged subsequently and increased to a final value of 0.0055. By contrast, the ionic and bridged/bidentate nitrate species were already observed within the first few minutes. At the end of the experiment, the ionic nitrate reached an area of 0.009, whereas for the bidentate/bridged nitrate a final area of 0.005 was observed. For none of the nitrate and nitrite species was a constant intensity observed during the experiment, indicating no saturation of the ceria sample. The similar temporal behavior of the nitrate/nitrite increase on one hand and the Ce-O/hydroxide decrease on the other suggests their reaction during NO_2 exposure. Further oxygen may be provided by the bulk, as indicated by the redshift of the F_{2g} feature. As soon as the consumption of surface oxygen slowed down, the redshift also became slower.

Fig. 5d depicts the breakthrough curves for NO and NO_2. Within the first 20 min nearly no NO or NO_2 could be observed, indicating complete storage of the provided NO_2. Afterwards NO broke through and increased to a concentration of 160 ppm. The NO breakthrough nearly coincided with the maximum of the nitrite intensity at 1292 cm^{-1}, indicating that during NO_2 exposure NO is formed and directly stored as nitrite. As a result NO starts to break through as soon as the adsorption sites for nitrite are saturated. The

NO_2 breakthrough started after 35 min of NO_2 exposure and increased to a concentration of 60 ppm at the end of the experiment. Since the NO_x outlet concentration did not reach the NO_2 inlet concentration, the ceria sample was not saturated even after 60 min of NO_2 exposure. After 1 h of NO_2 storage the NO_x storage capacity was determined to be 0.32 mmol/g.

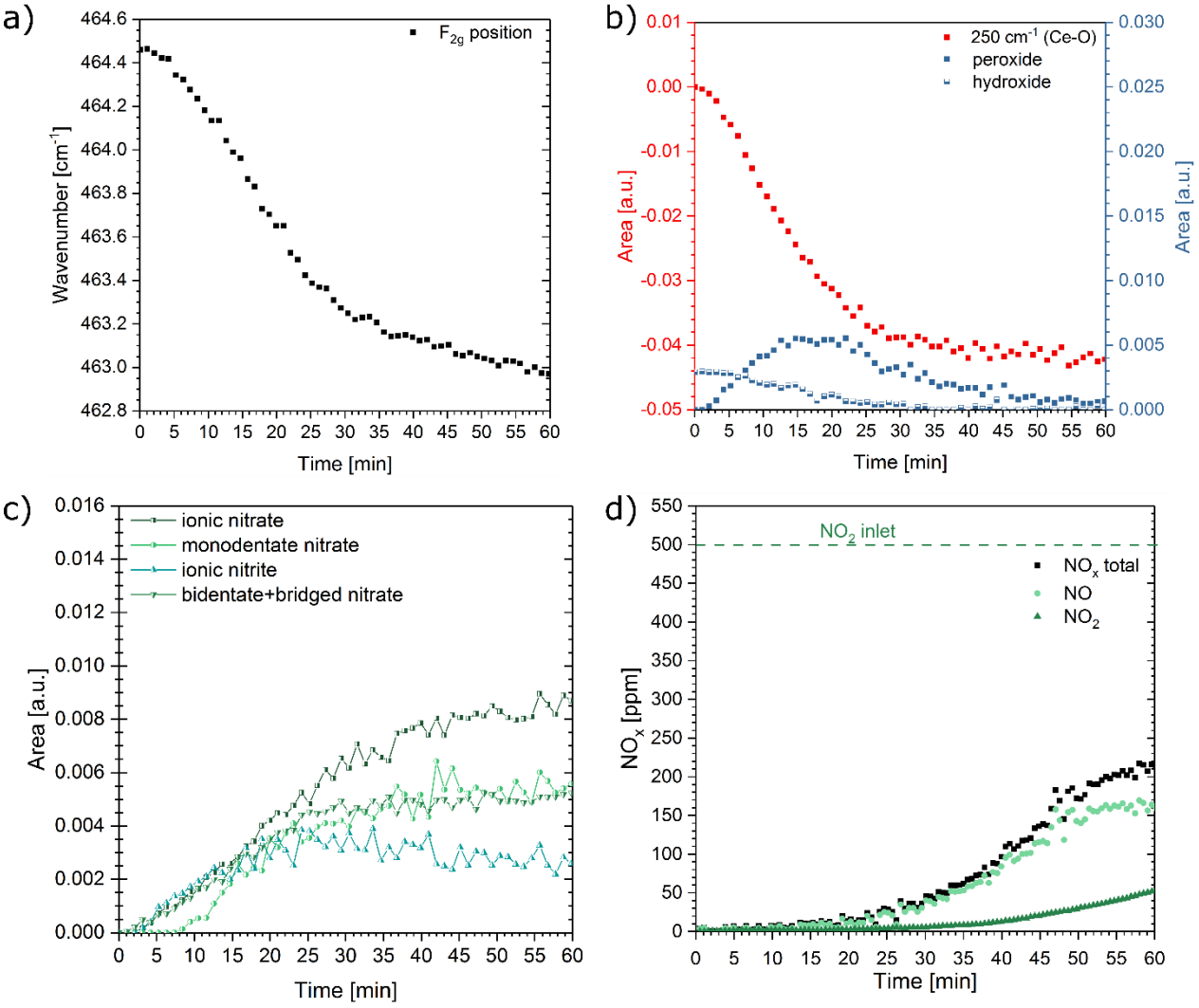

Fig. 5. Temporal evolution of (a) F_{2g} position, (b) Ce-O, peroxide, and hydroxide intensities, and (c) nitrite and nitrate intensities of oxidatively treated ceria upon NO_2 exposure with oxygen at 30°C. Fig. 5d depicts the outlet concentrations of NO and NO_2 obtained by FT-IR gas phase analysis, whereas the dashed line shows the NO_2 inlet concentration.

3.4 NO_2 storage with oxygen at 30°C after reductive treatment

Fig. 6a-c depicts the temporal evolution of characteristic ceria and nitrate/nitrite features of reductively treated ceria upon NO_2 exposure, as well as the NO and NO_2 concentration at the outlet (see Fig. 6d). The dashed line in Fig. 6d indicates the NO_2 inlet concentration.

Although ceria was reduced prior to NO_2 exposure, nearly no peroxides were observed during reaction. It should be mentioned that during reduction with hydrogen water was formed, which adsorbed on oxygen

vacancies at the surface and dissociated to hydroxides [53], resulting in fewer oxygen vacancies accessible to molecular oxygen to form peroxides. Furthermore, during NO_2 exposure hydroxides reacted with NO_2, forming nitrates, oxygen vacancies, and water (see eq. 2), which in turn adsorbed on the ceria surface, as indicated by a broad feature at around 3500 cm^{-1} (see Fig. S3). After about 20 min no more hydroxide was observed. The F_{2g} feature shifted by 1.4 cm^{-1} in total, showing a redshift of about 1 cm^{-1} within the first 20 min. A similar temporal behavior was observed for the intensity change of the Ce-O feature at 250 cm^{-1}. After about 35 min no further decrease in intensity was observed. Again, these findings are consistent with the consumption of surface oxygen and hydroxide during NO_2 storage accompanied by the diffusion of bulk oxygen to the surface leading to oxygen defect formation in the bulk.

Although ceria was reduced prior to NO_2 exposure, the type and amount of formed nitrate and nitrite species was similar to that of oxidatively treated ceria, indicating only a small influence of pretreatment on NO_2 storage. Upon NO_2 exposure initially only the formation of ionic nitrate and ionic nitrite was observed. Both species showed a similar formation rate within the first 10 min. Then the ionic nitrate feature further increased in a linear-like fashion and then, after about 25 min, slowed down reaching an area of 0.009 at the end of the experiment. The ionic nitrite showed a slower increase reaching a maximum after 18 min and subsequently decreased to an area of 0.002 indicating conversion of the species. The monodentate and bidentate/bridged nitrates were first observed after about 6 min showing a linear-like increase to an area of 0.0035 after 30 min and then a slower increase reaching a final value of 0.0045 after 60 min. Again, the intensity of the nitrate and nitrite species did not show a constant value at the end of the experiment, indicating that the ceria was not saturated.

No NO_x was observed at the outlet within the first 18 min. Then NO started to break through, followed by NO_2 after 30 min. However, the NO_2 inlet concentration was not reached even after 60 min of NO_2 storage, indicating that the maximum storage capacity was not reached. Again, the NO breakthrough coincided approximately with the maximum of the ionic nitrite, suggesting the saturation of nitrite adsorption sites. Furthermore, after about 45-50 min the NO concentration showed a maximum and subsequently decreased slowly. Meanwhile, the gradient of the NO_2 breakthrough increased gradually, indicating a decreasing re-oxidation of the ceria surface and hence NO_2 to NO conversion (see eq. 3). As could be shown by an experiment with a smaller amount of ceria, the decrease of NO breakthrough was followed by a fast increase of NO_2 concentration until the inlet concentration was reached and is therefore an indication that the sample is nearly saturated (see Fig. S4). After 1 h of NO_2 storage the NO_x storage capacity was determined to be 0.28 mmol/g.

3.5 NO/NO_2 storage with oxygen at 30°C after oxidative treatment

Fig. 7a-c depicts the temporal evolution of characteristic ceria, nitrate, and nitrite features after oxidative treatment upon NO and NO_2 exposure. Furthermore, Fig. 7d depicts the NO and NO_2 concentration at the outlet, while the dashed lines indicate the NO, NO_2, and total NO_x inlet concentrations.

Upon gas exposure peroxides emerged and reached a maximum within the first 10 min, followed by a slower decrease and disappearance after 55 min, indicating a fast reduction and re-oxidation of the ceria

surface. In contrast, the Ce-O feature at 250 cm^{-1} decreased in intensity followed by an intermediate increase after 30 min of gas exposure, suggesting the formation of new Ce-O sites by oxidation of the ceria surface. The F_{2g} feature redshifted about 1 cm^{-1} in total, whereas intermediately no shift was observed, coinciding with the intensity increase of the 250 cm^{-1} feature. The intermediately constant F_{2g} position may be rationalized by a pause of bulk oxygen diffusion to the surface as oxygen becomes available for the gas phase.

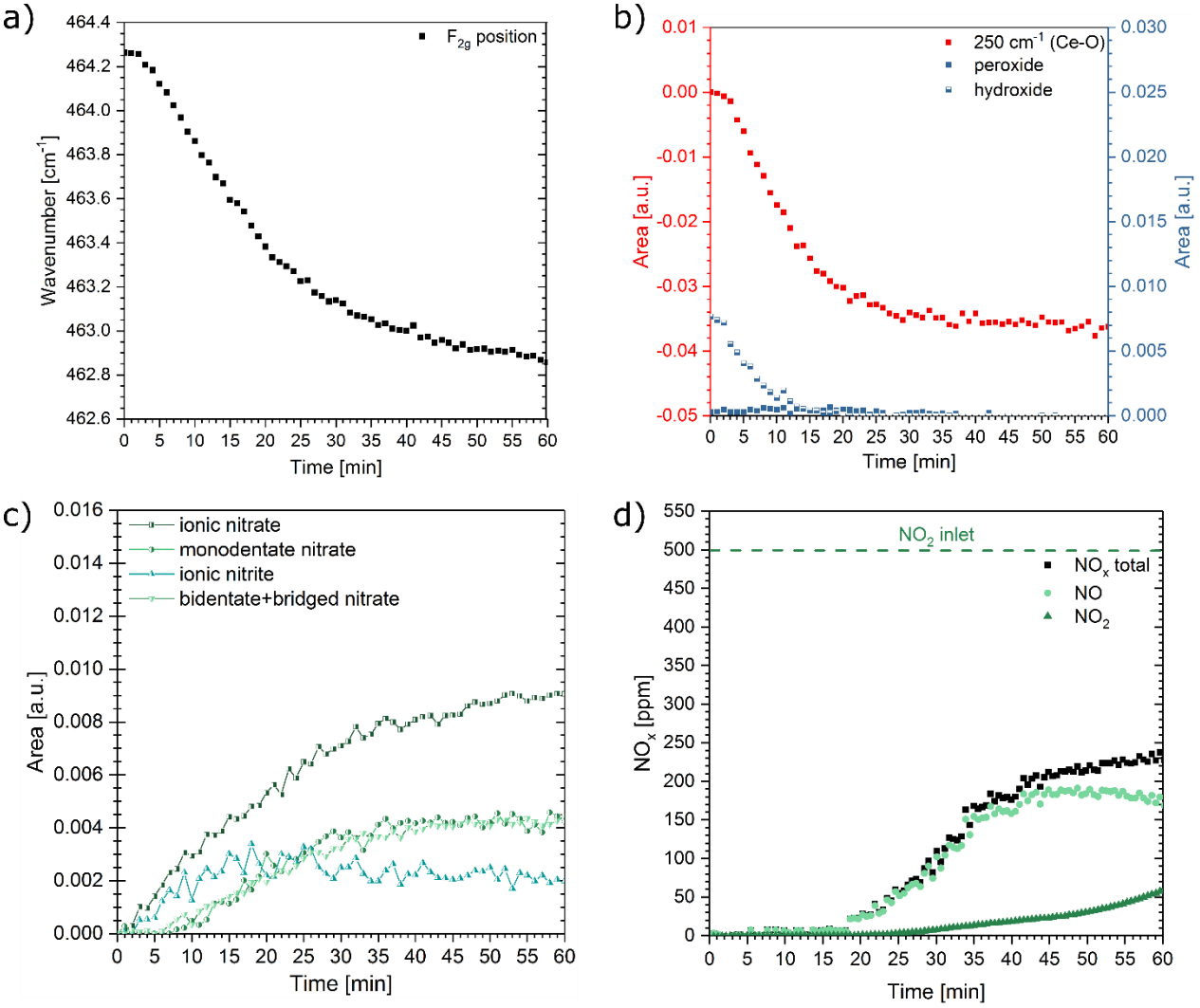

Fig. 6. Temporal evolution of (a) F_{2g} position, (b) Ce-O, peroxide, and hydroxide intensities, and (c) nitrite and nitrate intensities of reductively treated ceria upon NO_2 exposure with oxygen at 30°C. Fig. 6d depicts the outlet concentrations of NO and NO_2 obtained by FT-IR gas phase analysis, where the dashed line shows the NO_2 inlet concentration.

In contrast, the hydroxides continuously decreased to zero during the experiment. The fact that the intensity of the hydroxides decreased more slowly than the Ce-O intensity suggests that the reaction of NO_x with surface oxygen is preferred.

As can be seen in Fig. 7c, the NO_x adsorption behavior was dominated by the ionic nitrite, which emerged after 6 min of exposure and reached a maximum area of about 0.011 after 35-40 min. Within the first 20 min, no or only weak features of other species were observed. Subsequently, ionic and bidentate/bridged/monodentate nitrates were observed, reaching areas of 0.0075 and 0.0045, respectively. None of the nitrate or nitrite species reached a constant intensity, indicating ongoing reactions of NO_x species on the ceria sample.

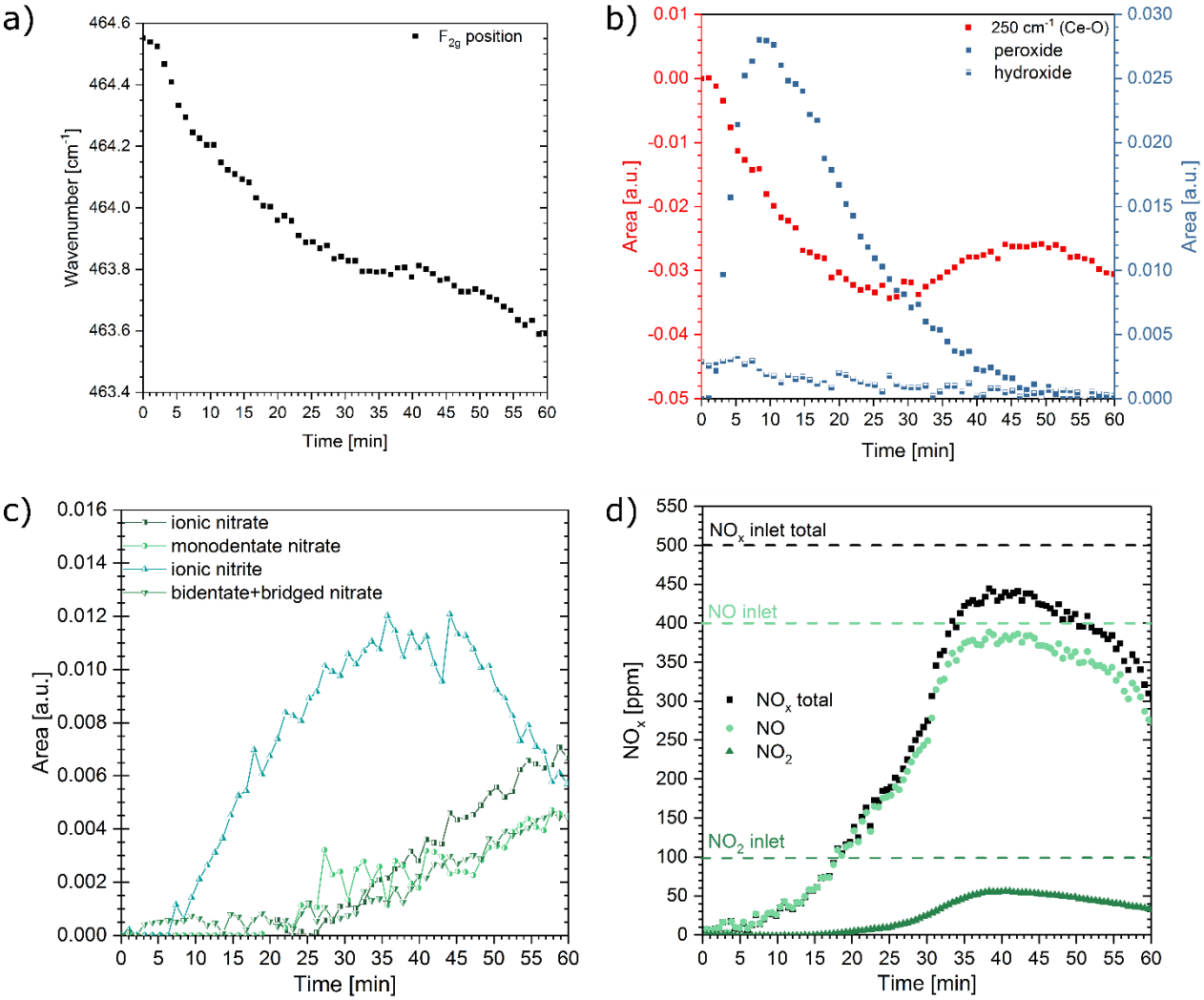

Fig. 7. Temporal evolution of (a) F_{2g} position, (b) Ce-O, peroxide, and hydroxide intensities, and (c) nitrite and nitrate intensities of oxidatively treated ceria upon NO/NO_2 exposure with oxygen at 30°C. Fig. 7d depicts the outlet concentrations of NO and NO_2 obtained by FT-IR gas phase analysis, whereas the dashed lines show the NO, NO_2 and NO_x total inlet concentration.

At the outlet of the reaction cell nearly no NO_x was observed within the first 8 min. Thereafter, the NO concentration increased showing an intermediate maximum concentration of 390 ppm after 35-40 min. A similar temporal behavior was observed for the NO_2 concentration increasing to a maximum concentration of 60 ppm. The decrease of NO_x concentration at the outlet coincided with the decrease of the ionic nitrite, suggesting that, after reaching a critical concentration, ionic nitrite reacted with NO_x from the gas phase to

give nitrate, resulting in a decrease of NO_x concentration and ionic nitrite intensity. After 60 min of exposure, the NO_x outlet concentration had not reached the sum of inlet concentrations and therefore the ceria sample was not saturated. After 1 h of NO_x storage the NO_x storage capacity was determined to be 0.24 mmol/g.

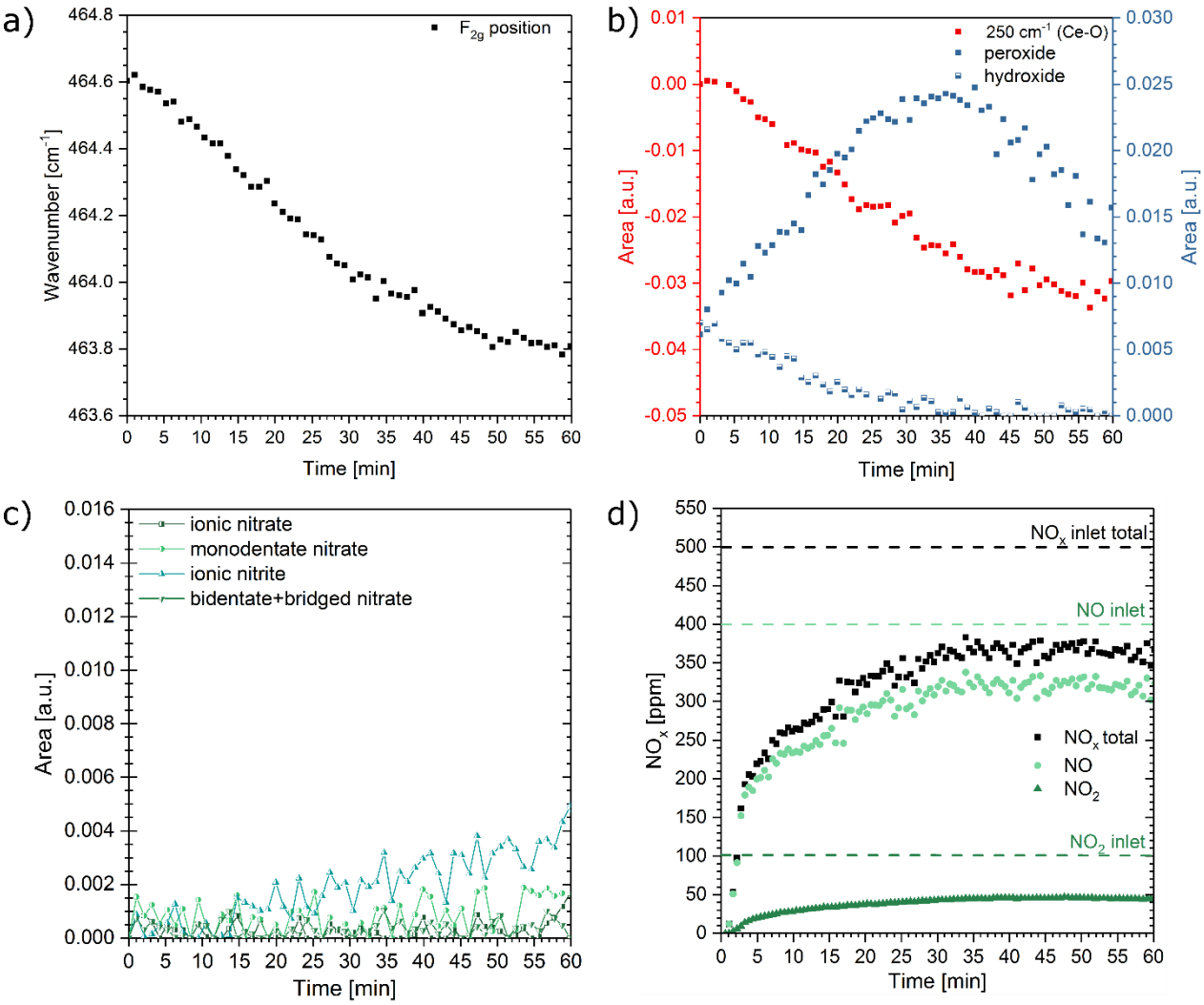

Fig. 8. Temporal evolution of (a) F_{2g} position, (b) Ce-O, peroxide, and hydroxide intensities, and (c) nitrite and nitrate intensities of reductively treated ceria upon NO/NO_2 exposure with oxygen at 30°C. Fig. 8d depicts the outlet concentrations of NO and NO_2 obtained by FT-IR gas phase analysis, while the dashed lines show the NO_x, NO_2, and NO inlet concentrations.

3.6 NO/NO_2 storage with oxygen at 30°C after reductive treatment

Fig. 8a-c depict the temporal evolution of characteristic ceria, nitrate, and nitrite features after reductive pretreatment and during NO and NO_2 exposure. Furthermore, Fig. 8d depicts the NO and NO_2

concentration at the outlet, while the dashed lines indicate the NO, NO_2, and NO_x total inlet concentrations.

The peroxide intensity reached a maximum after 35-40 min indicating an initial formation of surface defects and their subsequent partial healing. Upon NO_x exposure the Ce-O feature steadily decreased, but the decrease slowed down after about 45 min. For the 0.8 cm^{-1} redshift of the F_{2g} feature a similar temporal behavior was observed, pointing to a correlation between bulk and surface oxygen. For the hydroxide species, a continuous intensity decrease and disappearance after about 35 min was observed.

The reductive treatment resulted in a significantly lower formation rate of nitrate and nitrite upon NO_x exposure (see Fig. 8c). Nearly no nitrate was observed after 60 min. Only the ionic nitrite showed a significant increase, emerging after about 10 min and increasing subsequently to an area of about 0.004 after 60 min. As can be seen in Fig. 8d, the low formation rate of ionic nitrite resulted in a NO breakthrough within the first minutes of exposure. A NO_x concentration of 220 ppm was reached at the outlet after 5 min. Afterwards, the increase slowed down and a concentration of 370 ppm was observed after 35 min of reaction time, showing no further increase until the end of the experiment. Since the inlet concentration was not reached after 60 min NO_x exposure, the ceria sample was not saturated. After 1 h NO_x storage the NO_x storage capacity was determined to be 0.15 mmol/g.

3.7 NO_2 and NO storage without oxygen after oxidative treatment

To elucidate the influence of gas-phase oxygen, NO and NO_2 storage experiments were performed on oxidatively treated ceria at 30°C and 200°C without the presence of gas-phase oxygen.

Qualitatively, the NO_2 storage behavior without oxygen (see Fig. S5) resembled the behavior with oxygen (see Fig. 5). However, some differences were observed. The ionic nitrite intensity increased faster, so that it was more obvious that ionic nitrites were formed in the first place. The ionic nitrite intensity again reached a maximum after about 25 min of NO_2 exposure and subsequently decreased. The ceria was not saturated at the end of the experiment. After 1 h of NO_2 exposure the NO_x storage capacity was determined to be 0.36 mmol/g. Since no fundamental differences were observed with and without oxygen and the storage capacities had a similar magnitude, gas-phase oxygen does not seem to play a key role in NO_2 storage.

The NO storage experiment at 30°C without oxygen was performed for 3 h to make sure that no major changes occurred after 60 min exposure. Fig. S6a-c depicts the temporal evolution of characteristic ceria, nitrate, and nitrite features after oxidative treatment and upon NO exposure without oxygen. The NO and NO_2 outlet concentrations are shown in Fig. S6d. Upon gas exposure the peroxide area reached a maximum within 20 min of NO exposure, indicating an immediate reduction of the ceria surface. The continuous decrease of the hydroxide and Ce-O features suggests their consumption during NO exposure. The F_{2g} feature redshifted by 0.8 cm^{-1} in total without attaining a constant value after 3 h, and showed a temporal evolution of its position correlated with the temporal evolution of the Ce-O surface feature.

The NO_x adsorption behavior was dominated by ionic nitrite emerging after 20 min and strongly increasing within 100 min to its final area value. Therefore, in the absence of gas-phase oxygen, no conversion of the ionic nitrite was observed, indicating a key function of gas-phase oxygen for nitrite conversion consistent with the observation of Symalla *et al.* [33]. Besides ionic nitrite, initially a small amount of bidentate/bridged nitrate species was observed (see Fig. S6c), reaching a maximum area after 30 min. The ionic nitrate emerged after about 90 min of NO exposure showing a slow rise. Since the bidentate/bridged nitrate decreased slowly and no decrease of the ionic nitrite was observed, the increase of the ionic nitrate may be indicative of a conversion of the bidentate/bridged nitrate to ionic nitrate.

As depicted in Fig. S6d, the NO broke through within the first few minutes showing a NO outlet concentration of 420 ppm after 20 min and reaching the NO inlet concentration after about 140 min. No NO_2 was observed during the experiment. The NO_x storage capacity was determined to be 0.11 mmol/g after 1 h and 0.15 mmol/g after 3 h of exposure.

Wang *et al.* [19] and Martínez-Arias *et al.* [28] assumed that nitrite was converted with lattice oxygen of ceria to nitrate at temperatures above 100°C. Since no conversion of the nitrite species without oxygen was observed at 30°C, we also performed NO storage experiments without oxygen at 200°C to examine if lattice oxygen was involved in a reaction at higher temperatures (see Fig. S7).

While the peroxides shows only a very small intensity, the Ce-O feature was much more intense, but showed a significantly lower decline than for the reaction at 30°C. For the hydroxides no change in intensity was observed. The F_{2g} feature redshifted by only 0.1 cm^{-1} within the first 10 min and showed no change in position afterwards. All in all, at 200°C the characteristic ceria features showed noticeably weaker changes upon NO exposure than at 30°C. A similar behavior was also observed for the nitrate and nitrite species, indicating a lower stability at higher temperatures. Initially, ionic nitrite emerged, reached a maximum area after 12 min, and subsequently decreased at slower rate. The observed decrease in ionic nitrite intensity at 200°C suggests a conversion of ionic nitrite to nitrate. Consistent with this suggestion, an increase of ionic, monodentate, and bidentate/bridged nitrate were observed upon NO exposure at 200°C without oxygen. As it is proposed that no oxygen is present in the gas phase, the conversion of the ionic nitrite originates from the reaction of ionic nitrite with lattice oxygen.

At the outlet, nearly no NO was observed within the first 5 min. Afterwards, the NO concentration increased to the inlet concentration within 20 - 25 min indicating saturation of ceria for NO exposure without oxygen. The NO_x storage capacity in the absence of oxygen at 200°C was calculated to be 0.07 mmol/g, which is 37% lower than the value obtained in the absence of oxygen at 30°C.

3.9 NO_x desorption

Fig. 9 summarizes the NO_x storage capacities for NO_2 and NO/NO_2 storage into oxidatively and reductively treated ceria as well as the amounts of desorbed NO_x within 30-200°C, 200-400°C, and 400-500°C. In all experiments part of the NO_x desorbed at temperatures below 200°C. In case of NO_2 storage the desorbed amount at ≤200°C was 0.03 mmol/g independent of sample pretreatment corresponding to 9.4% (10.7%) of the stored NO_x for oxidatively (reductively) treated ceria. In contrast, for NO/NO_2 storage,

the desorption behavior strongly depends on pretreatment. Fig. 9 shows that in case of oxidative treatment the desorbed amount of NO_x at ≤200°C was 0.03 mmol/g corresponding to 4.2% of the stored NO_x, whereas in case of reductive treatment 0.09 mmol/g NO_x was detected at ≤200°C corresponding to 60% of the stored NO_x.

Likewise, within 200–400°C for NO_2 storage the pretreatment does not have a significant influence on the desorbed NO_x amounting to 0.20 mmol/g NO_x (62.5%) in case of oxidative treatment and 0.18 mmol/g NO_x (64.3%) in case of reductive treatment, respectively. However, for NO/NO_2 storage, again a strong dependence on pretreatment is observed. While in case of reductive treatment only 0.02 mmol/g NO_x (13.3%) was desorbed, oxidative treatment resulted in the detection of a large NO_x amount of 0.16 mmol/g (66.7%).

As shown in Fig. 9, within 400–500°C, NO_x is desorbed for all samples. For NO_2 storage the amount of desorbed NO_x was 0.06 mmol/g corresponding to 18.7% und 21.4% for oxidatively and reductively treated ceria, respectively. On the other hand, for NO/NO_2 exposure to oxidatively treated ceria 0.05 mmol/g NO*x* (20.8%) and in case of reductive pretreatment 0.02 mmol/g NO_x (13.3%) was desorbed.

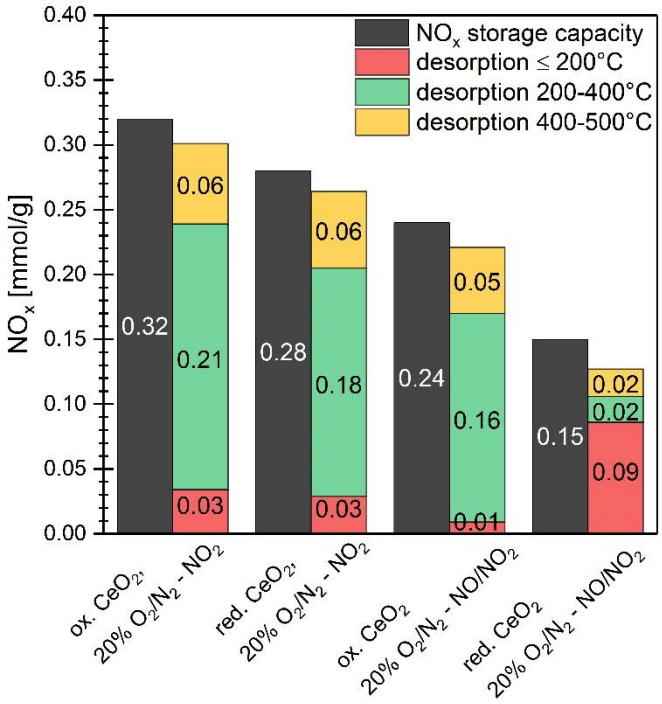

Fig. 9. NO_x storage capacities for NO_2 and NO/NO_2 storage into oxidatively and reductively treated ceria as well as the amounts of desorbed NO_x within 30-200°C, 200-400°C, and 400-500°C.

4. Discussion

4.1 Comparison of NO_2 and NO/NO_2 storage in ceria

Since gas-phase oxygen adsorbs on two electron defects forming peroxides and can therefore be used as an indication for surface oxygen vacancies, the peroxide intensities were traced during NO_x storage.

Furthermore, we investigated whether peroxide is an active oxygen species participating in reactions during NO_x storage. In all experiments an increase and subsequent decrease of the peroxide intensity was observed, indicating a dynamical behavior of the surface defects.

Comparing the temporal evolution of nitrate, nitrite, and peroxide features revealed no dependence of the nitrate and nitrite species on peroxides. Hence, peroxides are only a spectator and can be used as an indicator for surface oxygen vacancies. This assumption is supported by the observations during NO/NO_2 exposure at 30°C. While upon NO exposure with oxygen ionic nitrite was transformed to nitrate (see Fig. 7), during NO storage without oxygen no such transformation was observed (see Fig. S6). Consequently, for nitrite conversion activated gas-phase oxygen is needed. In both experiments peroxides were observed, showing a similar temporal intensity evolution. Therefore, peroxides can be excluded as active oxygen species for ionic nitrite transformation. Another possibility for an active oxygen species could be a superoxide. As was shown by Pushkarev *et al.* and Descorme *et al.* superoxide is thermally the most unstable oxygen species, therefore leading to a high reactivity [44, 54]. Furthermore, in literature the interaction of nitrite with superoxide as an active oxygen species was supposed to be responsible for the transformation of nitrite to nitrate [27, 28]. However, Martínez-Arias *et al.* conducted experiments in vacuum [28], which affects the state of ceria and consequently the NO_x storage mechanism during reaction. Although superoxides are accessible by Raman spectroscopy, no superoxides were detected during our experiments. Thus, in this work an interaction of nitrite with superoxide could not be confirmed.

Table 2 summarizes the results for the NO_x storage capacity, the F_{2g} shift, the areas of the nitrate and nitrite species, as well as the decrease in Ce-O and hydroxide area after 1 h of NO_x exposure. Comparing the NO_2 experiments only small differences in the amount of nitrate and nitrite species were observed, indicating that NO_2 storage is largely independent of pretreatment and the presence of gas-phase oxygen. A similar behavior was observed for the NO_x storage capacity, which was not much affected by the pretreatment. For the NO_2 exposure with oxygen, a NO_x storage capacity of about 0.3 mmol/g was reached after 1 h (see Table 2). The NO_2 storage without oxygen gave an even slightly higher NO_x storage capacity (0.36 mmol/g after 1h of NO_2 exposure), indicating no need of gas-phase oxygen for NO_2 storage as NO_2 can act as an oxygen source. After 2 h of 500 ppm NO_2/N_2 exposure the ceria was saturated and a NO_x storage capacity of 0.52 mmol/g was reached (not shown). Azambre *et al.* investigated the NO_x storage capacity of a ceria with a specific surface area of 284 m²/g. After 300 min of 1000 ppm NO_2/Ar exposure they observed a NO_x storage capacity of about 60 mg/g NO_2, which is by a factor of 2.5 higher than the NO_x storage capacity observed in this work (24 mg/g) [31]. However, taking into account the 4 times higher surface area of their ceria material the NO_x storage capacity reached in this work compares favorably with the reported value. Considering the adsorbed NO_x species upon NO_2 exposure the temporal evolution of the nitrate and nitrite species showed small differences on pretreatment. After reductive treatment ionic nitrite reached only a maximum area of 0.003 (see Fig. 6), compared to 0.004 after oxidative treatment (see Fig. 5). After 1 h of NO_2 exposure the amount of nitrite was slightly lower as well, indicating a lower formation rate of ionic nitrite on defective ceria. By considering eq. 4, a reduction of the ceria surface is expected to result in a higher amount of nitrite.

However, the contrary was the case and therefore eq. 4 was not confirmed by Raman spectroscopy, implying that nitrite was primarily formed by the reaction of NO with surface oxygen. On the contrary, it should be noted that Raman spectroscopy could not observe all nitrite species so that no conclusion is drawn concerning the existence of eq. 4. However, based on DFT calculations, Nolan *et al.* showed that adsorption of NO_2 onto an oxygen vacancy results in the formation of nitrite as an intermediate adsorption structure decomposing subsequently to NO and reoxidizing the ceria surface (see eq. 3) [29]. As shown in Fig. 6, for the reductively treated ceria as compared to the oxidatively treated ceria shown in Fig. 5, a higher formation rate of ionic nitrate was observed at the beginning, as well as a higher level and a faster decrease in hydroxide intensity, indicating that ionic nitrate was formed by the reaction of NO_2 with hydroxide.

By contrast, upon NO/NO_2 exposure the NO_x storage capacity and the amount of nitrate and nitrite species were strongly dependent on the pretreatment and the presence of gas-phase oxygen (see Table 2). While a NO_x storage capacity of 0.24 mmol/g was reached after 1 h of NO/NO_2 exposure for the oxidatively treated ceria, it decreased to 0.15 mmol/g for the reductively treated ceria and further to 0.11 mmol/g upon exposure without oxygen after oxidative treatment. Long-time $NO/NO_2/N_2$ adsorption resulted in a NO_x storage capacity of 0.16 mmol/g (not shown), which is 4 times smaller than the NO_x storage capacity (0.67 mmol/g) observed during 500 ppm NO/Ar exposure by Azambre *et al.* [31]. However, taking into account the distinct surface areas of their ceria samples the observed NO_x storage capacity is in good agreement with the reported result. Therefore, gas-phase oxygen as well as ceria lattice oxygen play an important role during NO/NO_2 storage. In the presence of oxygen at 30°C predominantly ionic nitrite was observed within the first 25 min (see Fig. 7). Afterwards, a significant amount of nitrate emerged followed by a decrease of ionic nitrite. However, in the absence of oxygen only an increase of the ionic nitrite intensity and nearly no nitrates were observed (see Fig. S6), implying that nitrates were primarily formed by reaction of ionic nitrite with gas-phase oxygen. Furthermore, the decrease of nitrite species coincided with the decrease of NO and NO_2 outlet concentrations (see Fig. 7), indicating a participation of gas-phase NO_x in the nitrite transformation reaction. As a consequence, two new reaction pathways are postulated for nitrite conversion upon NO/NO_2 exposure at 30°C:

$$Ce^{3+} - NO_2^- + Ce^{3+} - \square - Ce^{3+} + O_2 + NO \rightarrow Ce^{3+} - NO_3^- + Ce^{3+} - NO_2^- + Ce^{4+} \quad (17)$$

$$Ce^{3+} - NO_2^- + Ce^{3+} - \square - Ce^{3+} + O_2 + NO_2 \rightarrow Ce^{3+} - NO_3^- + Ce^{3+} - NO_3^- + Ce^{4+} \quad (18)$$

As a simultaneous interaction of two gas-phase species with two surface species is unlikely, a sequence of steps is expected. A feasible scenario might involve reaction of oxygen with ionic nitrite followed by either reoxidation of the oxygen vacancy or reaction with gas-phase NO_x. However, our experiments do not allow a distinction of the individual processes; therefore, we combined these processes in one equation.

Table 2

Areas of ionic nitrate, ionic nitrite, monodentate, and bidentate/bridged nitrate, Ce-O and hydroxide peaks, as well as the NO_x storage capacity and F_{2g} shift after 60 min of NO_x storage, dependent on treatment and the presence or absence of gas-phase oxygen.

Experiment	**NO_x storage capacity (±0.02) [mmol/g]**	**F_{2g} shift (±0.1) [cm^{-1}]**	**Hydroxide Area[a] (±0.0003) [a.u.]**	**Ce-O (250 cm^{-1}) Area[a] (±0.004) [a.u.]**	**Ionic nitrate Area (±0.0005) [a.u.]**	**Bridged & bidentate nitrate Area (±0.0003) [a.u.]**	**Monodentate nitrate Area (±0.001) [a.u.]**	**Ionic nitrite Area (±0.001) [a.u.]**
Ox. CeO_2, 20% O_2 – NO_2, 30°C	0.32	-1.5	-0.0030	-0.042	0.0090	0.0050	0.0055	0.0025
Red. CeO_2, 20% O_2 – NO_2, 30°C	0.28	-1.4	-0.0075	-0.036	0.0090	0.0045	0.0045	0.0020
Ox. CeO_2, 20% O_2 – NO/NO_2, 30°C	0.24	-1.0	-0.0030	-0.031	0.0075	0.0045	0.0045	0.0060
Red. CeO_2, 20% O_2 – NO/NO_2, 30°C	0.15	-0.8	-0.0070	-0.032	0.0017	0.0005	0.0017	0.0040
Ox. CeO_2, N_2 – NO_2, 30°C	0.36	-1.5	-0.0025	-0.042	0.0080	0.0050	0.0050	0.0020
Ox. CeO_2, N_2 – NO, 30°C	0.11	-0.8	-0.0030	-0.024	0.0008	0.0005	0.0000	0.0065
Ox. CeO_2, N_2 – NO, 200°C	0.07	-0.1	-0.0000	-0.007	0.0020	0.0008	0.0005	0.0010

[a] Please note that for Ce-O and hydroxide negative values are given corresponding to a decrease in area.

Wang *et al.* [19] and Martínez-Arias *et al.* [28] predicted a transformation of nitrite species to nitrate with lattice oxygen from ceria at temperatures above 100°C (see eq. 5). Such a transformation was not observed at 30°C (see Fig. S6), but at 200°C (see Fig. S7). Therefore, for the reaction of the nitrite species with lattice oxygen an activation energy needs to be overcome.

The reductive treatment of ceria prior to NO/NO_2 exposure resulted in a lower formation rate of ionic nitrite (see Fig. 8). The observed formation of peroxides is attributed to oxygen diffusion to the surface. Even though oxygen was present, it was not able to re-oxidize the ceria surface effectively. As surface oxygen is needed for NO storage (see eq. 8), the nitrite formation rate consequently slowed down. Therefore, after reductive treatment followed by 1 h of NO/NO_2 exposure solely nitrite was observed, as the critical ionic nitrite concentration for transformation to nitrate was not reached by then. The observed dependence of the NO_x storage capacity upon NO/NO_2 exposure on the pretreatment is consistent with the observations of Theis and Lambert [3], as well as the higher storage capacity for NO_2 storage.

Prior to NO_x exposure hydroxides were observed on all samples. Upon NO_x exposure the hydroxide intensity decreased to zero except for the experiment at 200°C, indicating a consumption according to eqs. 2 and 9. Since the decrease in hydroxide intensity was faster upon NO_2 exposure, the hydroxide reacted preferably with NO_2, forming nitrates. Even though the amount of hydroxides was higher after reductive treatment (see Table 2), the NO_x storage capacity was lower, indicating that eqs. 2 and 9 contribute only to a small extent to the overall NO_x storage capacity and therefore hydroxide is a negligible reactant in NO_x storage.

Furthermore, for all samples a decrease in the Ce-O intensities was observed, indicating a consumption of oxygen according to eqs. 1 and 8. Moreover, the decrease in Ce-O intensity was greater the higher the NO_x storage capacity, indicating the importance of Ce-O sites for NO_x storage. However, the Ce-O decrease after 60 min of NO/NO_2 exposure was comparable for reductive and oxidative treatment although different NO_x storage capacities were observed. This behavior can be explained as follows: As shown by Fig. 7b, an intermediate increase of Ce-O intensity was measured for the oxidatively treated ceria, and consequently new Ce-O sites were formed intermediately. Thus, while the observed overall decrease of the Ce-O feature after 60 min of NO/NO_2 exposure was lower for the oxidatively treated than for the reductively treated ceria, the overall consumption of Ce-O sites for the oxidatively treated ceria was higher.

During NO_x exposure the F_{2g} feature redshifted and hence indicated a reduction of the ceria bulk (see Table 2). Using DFT+U calculations Schilling *et al.* found a relation between the stoichiometry $CeO_{2-\delta}$ and the F_{2g}-shift ($\Delta\omega$) of $\delta = 0.024 \pm 0.005\ \Delta\omega/cm^{-1}$.[55] However, since the stoichiometry prior to NO_x exposure is not known, only changes in stoichiometry but no absolute stoichiometry of ceria after NO_x storage can be given. Moreover, upon NO_x exposure at 30°C the F_{2g} redshift strongly resembled the temporal evolution of the Ce-O decrease at 250 cm^{-1} (see Fig. 10). NO/NO_2 storage after oxidative treatment is an exception. In this case, at the time when the intermediate increase of the Ce-O feature at 250 cm^{-1} was observed, the redshift of the F_{2g} feature paused, persisting as long as the increase of the Ce-O feature at 250 cm^{-1} (see Fig. 7). Based on this finding we conclude that diffusion of bulk oxygen to

the surface and consequently bulk oxygen vacancy formation was only observed as long as Ce-O sites were consumed by NO_x adsorption. Once new Ce-O sites were formed by reaction with gas-phase oxygen, the diffusion stopped. Hence, the formation of oxygen vacancies in the bulk correlated with the consumption of Ce-O sites at the surface. Furthermore, a correlation between the F_{2g} shift and NO_x storage capacity was observed. The higher the amount of stored NO_x, the larger the observed redshift (see Table 2) and, as mentioned above, the amount of consumed Ce-O sites. This observation is in turn consistent with the observation that the F_{2g} redshift correlated with the Ce-O decrease. Consequently, most of the NO_x was stored by reaction with Ce-O sites and eqs. 1 and 8 represent the dominant reaction pathways.

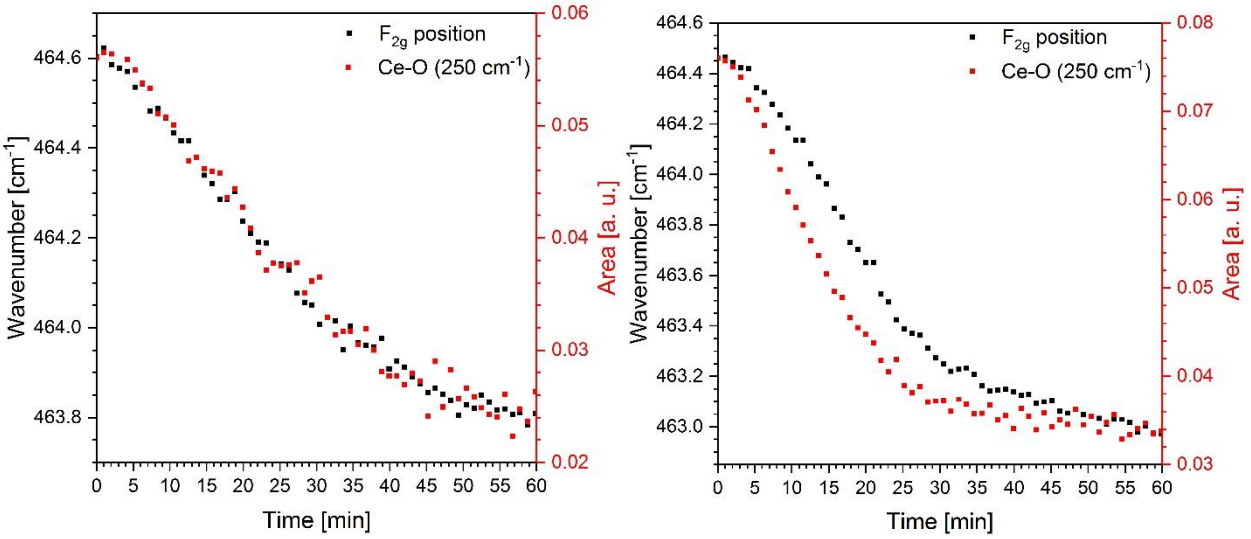

Fig. 10. Correlation of the temporal evolution of the F_{2g} position and the Ce-O intensity at 30°C after (left) reductively treated ceria upon NO/NO_2 exposure with oxygen (right) oxidatively treated ceria upon NO_2 exposure with oxygen.

In previous studies, NO and NO_2 storage in ceria at low temperatures (≤200°C) has been investigated by DRIFT spectroscopy [27, 31, 35, 56]. After NO/N_2 adsorption at 30°C, Zhang *et al.* observed monodentate, bidentate, and bridged nitrate as well as *trans*- and *cis*-hyponitrites. When ceria was reduced prior to NO adsorption, the intensity of nitrates and hyponitrites was lower and NO^- was detected. NO_2/N_2 adsorption on ceria resulted in the formation of the same nitrate and hyponitrite species, although the intensities were larger than after NO adsorption [56]. By contrast, Philipp *et al*. detected not only the formation of nitrates and hyponitrites, but also different nitrites during NO/N_2 adsorption on ceria at 50°C. In particular, the intensities of the nitrites were larger than those of the nitrates. In the presence of oxygen, new nitrate signals were observed, whereas the nitrite species at 1411 cm^{-1} could not be detected anymore. Furthermore, Philipp *et al*. observed a nitrite transformation to nitrate only upon $NO/O_2/N_2$ exposure at 200°C, whereas at 50°C no nitrite transformation occurred [35]. However, upon NO_2/Ar and NO/O_2/Ar exposure in ceria rich ceria-zirconia catalysts nitrite transformation was observed already at 30°C [27, 31]. In both experiments, the nitrite species at about 1180 cm^{-1} was the main feature observed

during the first minutes. After reaching a maximum intensity the nitrite intensity decreased while nitrates increased. Moreover, the NO_x storage was accompanied by a decrease of hydroxide intensity indicating a reaction of NO_x with surface OH groups [27, 31]. Depending on reaction conditions, using DRIFT spectroscopy also adsorbed N_2O or the formation of N_3^- was observed during NO_x exposure [30, 31]. When ceria was reduced prior to NO_x storage a broad adsorption band at about 2120 cm^{-1} was detected originating from a $^2F_{5/2} \rightarrow {}^2F_{7/2}$ forbidden electronic transition. Thus, while DRIFT spectroscopy enables the detection of a larger number of different NO_x species on ceria than Raman spectroscopy, the separation and assignment of signals is complicated by the amount of observed signals, leading to controversial assignments in literature [30]. The NO_x species observed by DRIFT spectroscopy do not necessarily coincide with those observed by Raman spectroscopy. In fact, DRIFT spectroscopy detected no nitrite transformation on pure ceria at 30°C, whereas Raman spectroscopy provided an indication on nitrite to nitrate transformation. Generally, DRIFT spectroscopy is more sensitive to the surface and therefore to adsorbates or hydroxyls on the ceria surface. On the other hand, the participation of the bulk is not considered since bulk properties are not directly accessible. As shown by the shift of the F_{2g} signal and the increase of the defect signal at 595 cm^{-1} in Raman spectra, NO_x storage in ceria proceeds not only on the ceria surface but also in the bulk, as oxygen for NO_x storage is provided by diffusion of oxygen ions from the bulk to the surface restoring Ce-O surface sites. In addition, Raman spectra provide direct evidence of the involvement of Ce-O surface sites for NO_x storage so far not accessible by other spectroscopic methods. As their amount strongly influences the NO_x storage capacity, these Ce-O sites play an important role for NO_x storage (see Table 2). Based on previous DRIFT spectra, hydroxides were discussed as NO_x adsorption sites resulting in nitrates and nitrites [27, 31]. In this work it is shown, that hydroxides play a negligible role in NO_x storage. Furthermore, the participation of superoxides in NO_x storage has been proposed in previous studies [27, 28]. However, by Raman spectroscopy both superoxides and peroxides can be detected but neither superoxides nor peroxides could be confirmed as active oxygen in NO_x storage in the present study.

Based on our results, storage mechanisms for NO and NO_2 in ceria are postulated (see Table 3). In Table 3, the reaction pathways are arranged in descending order of contribution and reaction speed.

4.2 NO_2 storage mechanism

Upon NO_2 exposure after oxidative treatment, an increase of the nitrite species was observed initially (see Fig. 5 and S4). Since reduction of the ceria surface and therefore formation of surface oxygen vacancies resulted in a smaller amount of nitrite (see Table 2), the adsorption of NO_2 on oxygen vacancies (eq. 4) is not considered a preferential pathway to nitrite. Likewise, a larger amount of hydroxides did not result in a larger amount of nitrites (see Table 2). This strongly suggests that nitrite is preferentially formed on Ce-O sites. However, the only reaction pathway to form a nitrite on a Ce-O site is by adsorption of NO (eq. 8) and consequently NO has to be formed in the first place. NO can be formed according to eqs. 3, 6, and 7. As at the beginning no nitrite is present, NO has to be formed by oxidation of the ceria surface with NO_2 (eq. 3). Thus, in the first step NO_2 reacts with surface vacancies, forming Ce-O sites and NO (eq. 3). Then

NO reacts on Ce-O sites to give nitrite (eq. 8). Furthermore, as the nitrite increases faster than the nitrate species, both reactions (i.e., eqs. 3 and 8) have to be very fast. After reductive treatment a slower increase of the nitrite feature was observed, which is consistent with the smaller amount of Ce-O sites present at the beginning. Therefore, the reaction of NO with Ce-O sites slowed down (eq. 8).

As the next step, the intensities of ionic nitrate and bidentate/bridged nitrate increased. A faster increase of the ionic nitrate was observed for reductively treated ceria as compared to oxidatively treated ceria. Furthermore, on the reductively treated ceria a greater amount of hydroxide was observed, which also decreased faster after reductive pretreatment compared to oxidative pretreatment. Consequently, the reaction of NO_2 with hydroxide resulted in the formation of ionic nitrate, oxygen vacancies, and water (eq. 2). The presence of adsorbed water in turn was proved spectroscopically (see Fig. S3).

Since adsorption of water on an oxygen vacancy is accompanied by water dissociation, resulting in the formation of two hydroxides [53], and only a decrease in hydroxide intensity was observed, water was probably adsorbed on a cerium atom adjacent to an oxygen vacancy. One hydrogen of the water molecule may then form a hydrogen bridge bond to a neighboring oxygen in the ceria lattice [53]. As a larger amount of hydroxides did not result in a larger NO_x storage capacity, the reaction pathway described in eq. 2 is not considered to play a key role for NO_x storage. Furthermore, the amount of ionic nitrate formed was independent of the amount of hydroxides (see Table 2). We conclude that ionic nitrate was also formed by reaction of NO_2 with Ce-O sites (see eq. 1). The reaction of NO_2 with Ce-O sites also resulted in the formation of monodentate and bidentate/bridged nitrate.

As oxygen vacancies were formed during the reaction of NO_2 with hydroxide, gas-phase oxygen was able to adsorb on these vacancies, forming peroxides (eq. 19). On the other hand, the formation of oxygen vacancies on the surface resulted in a diffusion of lattice oxygen from the bulk to the surface, causing a lattice expansion as a result of oxygen vacancy formation in the bulk. Hence, the lattice expansion leads to the observed redshift of the F_{2g} feature.

If sufficient nitrite is available on the ceria surface, nitrite can be oxidized to nitrate by NO_2 (see eq. 6). As could be shown by NO storage with and without oxygen (see Fig. 7 and 9), a transformation of nitrite by lattice oxygen does not proceed at 30°C (eq. 5) and can therefore be neglected at low temperatures. Furthermore, the transformation of nitrite could result in ionic, monodentate, or bidentate/bridged nitrate, based on the observed formation of these species during NO storage with oxygen (see Fig. 7). As long as Ce-O sites were accessible for NO adsorption, NO formed according to eq. 6 adsorbed on surface oxygen, forming nitrite (eq. 8). Once the Ce-O sites for nitrite formation were nearly consumed after about 20–25 min the NO started to slip through at the outlet and the nitrite intensity decreased (see Fig. 5 and 6).

As NO_2 is a strong oxidizer and can heal defects, the pretreatment had no significant impact on the NO_2 storage and NO_x storage capacity.

4.3 NO storage mechanism

As upon NO/NO_2 exposure no characteristic NO_2 storage behavior was observed (compare Fig. 7 and 5) and the behavior at the beginning was similar to the NO storage without oxygen (compare Fig. 7 and 9), we concluded that the NO/NO_2 storage was strongly dominated by the NO storage behavior. Consequently, a NO storage mechanism was postulated.

Upon NO exposure (see Fig. S6 and S7) and NO/NO_2 exposure (see Fig. 7 and 8) predominantly ionic nitrite was observed. Since NO acts as a reducing agent and O_2 is not a strong oxidizing agent, the pretreatment had a significant impact on the NO/NO_2 storage and therefore of the NO_x storage capacity. After reductive treatment the amount of ionic nitrite was significantly lower. Therefore, oxygen vacancies are obstructive for NO storage and NO reacts predominantly on Ce-O sites (eq. 8).

Furthermore, even in the absence of NO_2, a decrease of the hydroxide features was observed (see Fig. S6), indicating a reaction of NO with hydroxides (eq. 9). However, the reaction of NO with hydroxides was significantly slower than the reaction of NO_2 with hydroxides (see Fig. S6 and S5). The resulting water again adsorbed on the ceria surface. Since either no NO_2 or only a small amount was present during NO exposure, the oxygen vacancies were not re-oxidized and gas-phase oxygen could adsorb on these, giving rise to peroxides. Consequently, a significantly higher amount of peroxides originated upon NO exposure as compared to NO_2 exposure (see Fig. 7, 9 and 5). The formation of oxygen vacancies resulted again in a lattice expansion and a redshift of the F_{2g} feature caused by the diffusion of oxygen ions from the bulk to the surface.

After the amount of ionic nitrites reached a critical concentration, a transformation of nitrite occurred and ionic, monodentate, and bidentate/bridged nitrates were formed (see Fig. 7). However, the transformation was only observed in the presence of oxygen (see Fig. 7 and 9). As the amount of peroxides had no influence on the kinetics of the nitrite transformation, the activated oxygen species is not a peroxide. Furthermore, oxygen activation resulted in a re-oxidation of the ceria surface (eq. 20) and therefore in an intermediate increase of the Ce-O feature [57]. Moreover, the decrease of the nitrite feature was accompanied by an increased consumption of NO_x in the gas phase. This behavior was only observed in the presence of oxygen, thus describing new reaction pathways (eqs. 17 and 18). Once the temperature was increased, the mobility of lattice oxygen also increased, resulting, even in the absence of gas-phase oxygen, in the transformation of ionic nitrite to nitrate by lattice oxygen (see Fig. S7). Therefore, at higher temperatures no oxygen is needed for the transformation of nitrite. However, at higher temperatures, due to the lower thermal stability of nitrites and nitrates, less NO_x was stored.

Table 3

NO_2 and NO storage mechanisms in ceria.

NO_2 storage mechanism	
	(3)
	(8)
	(1)
	(2)
$-\mathrm{Ce^{3+}} + \mathrm{O_2} \rightarrow \mathrm{Ce^{4+}} - \mathrm{O_2^{2-}} - \mathrm{Ce^{4+}}$	(19)
	(6)
NO storage mechanism	
	(8)
	(9)
$-\mathrm{Ce^{3+}} + \mathrm{O_2} \rightarrow \mathrm{Ce^{4+}} - \mathrm{O_2^{2-}} - \mathrm{Ce^{4+}}$	(19)
$-\mathrm{Ce^{3+}} + \mathrm{O_2} \rightarrow 2\,\mathrm{Ce^{4+}} - \mathrm{O^{2-*}} - \mathrm{Ce^{4+}}$	(20)
$\mathrm{Ce^{3+}} - \mathrm{NO_2^-} + \mathrm{Ce^{3+}} - \square - \mathrm{Ce^{3+}} + \mathrm{O_2} + \mathrm{NO} \rightarrow \mathrm{Ce^{3+}} - \mathrm{NO_3^-} + \mathrm{Ce^{3+}} - \mathrm{NO_2^-} + \mathrm{Ce^{4+}}$	(17)
$\mathrm{Ce^{3+}} - \mathrm{NO_2^-} + \mathrm{Ce^{3+}} - \square - \mathrm{Ce^{3+}} + \mathrm{O_2} + \mathrm{NO_2} \rightarrow \mathrm{Ce^{3+}} - \mathrm{NO_3^-} + \mathrm{Ce^{3+}} - \mathrm{NO_3^-} + \mathrm{Ce^{4+}}$	(18)
	(5)

4.4 NO_x desorption

The NO_x desorption was investigated to gain insight into the stability of the formed nitrite and nitrate species. The desorbed NO_x was analyzed within the temperatures ranges 30-200°C, 200-400°C, and 400-500°C. Regarding technical applications it is desirable to store the NO_x during cold start at low temperatures and to release it at temperatures ≥200°C under lean conditions, where the SCR catalyst shows activity. Previous studies have reported on the desorption of NO_x from ceria after NO_x exposure at 120°C showing more NO_x desorption at <350°C (~55%) as compared to 350-500°C (~30%) [14]. However, the influence of ceria pretreatment on NO_x desorption behavior was not studied.

Fig. 9 shows that the amount of desorbed NO_x at ≤200°C is at a comparably low level for NO_2 storage and NO/NO_2 storage after oxidative treatment, whereas reductive treatment leads to desorption of 60% of the NO_x. This large amount of desorbed NO_x can be explained by the fact that during NO/NO_2 exposure to reductively treated ceria primarily nitrites are formed (see Fig. 8), which also desorb at lower temperatures due to their weaker interaction with ceria as compared to nitrates [14]. On the other hand, in case of NO/NO_2 exposure to oxidatively treated ceria, nitrite can be oxidized to nitrate during storage (Fig. 7) demonstrating that an oxidative pretreatment is highly beneficial to keep the amount of desorbed NO_x at ≤200°C low.

For NO_2 storage and NO/NO_2 storage after oxidative treatment most of the stored NO_x is desorbed within 200-400°C (62-67%) in contrast to NO/NO_2 storage after reductive treatment, for which only little NO_x desorption is detected within this temperature range (13%). The observed variation in NO_x desorption

behavior can thus be rationalized by the different amounts of nitrites and nitrates present after the NO_x storage experiments as well as the differences in thermal stability of nitrites and nitrates. In fact, our experiments show that NO_2 storage and/or oxidative treatment favor the formation of nitrates due to direct NO_2 storage or conversion of nitrites into nitrates, whereas NO/NO_2 exposure into reductively treated ceria leads primarily to nitrite formation. Thus, for the studied ceria material the desired characteristic of PNAs to desorb NO_x within 200-400°C would be best fulfilled for NO_2 storage and NO/NO_2 storage into oxidatively treated ceria.

It should be mentioned that at a temperature of 400°C the total amounts of desorbed NO_x were about 75 und 73% for NO_2 storage in oxidatively und reductively treated ceria, respectively, and about 71% for NO/NO_2 storage. Thus ceria was not fully regenerated at a temperature of 400°C owing to the presence of stable NO_x species.

5. Conclusion

In this study, the NO_2 and NO storage mechanism at 30 °C in ceria was investigated using Raman spectroscopy in combination with FT-IR gas phase spectroscopy. Proposed reaction pathways were spectroscopically investigated and critically discussed. Furthermore, based on our findings new reaction pathways are postulated.

The influence of defects on the NO_x storage was investigated by applying an oxidative or a reductive treatment prior to NO_x exposure. In the case of NO_2 exposure the treatment had no significant effect on the NO_x storage capacity, since NO_2 is a strong oxidizing agent and rapidly re-oxidized the ceria surface, forming new Ce-O sites and NO, which in turn adsorbed on the ceria surface. By contrast, in the case of NO exposure the pretreatment had a dramatic effect, resulting in a 38%-lowered NO_x storage capacity.

Raman spectra reveal evidence of the participation of Ce-O surface sites not observed previously by other spectroscopic methods. As shown in this study, these Ce-O sites on the ceria surface play a key role for NO_x storage, since NO_x is predominantly stored by their reaction with NO and NO_2 (see eqs. 1 and 8). Therefore, the ability of cerium to change oxidation state and accordingly the formation of defects is crucial for NO_x storage. By contrast, a higher amount of oxygen defects prior to NO_x exposure resulted in a lower NO_x storage capacity. Consequently, the existence of oxygen defects had a counter-productive effect on NO_x storage as long as no suitable oxidizing agent was present to heal them. Besides, a higher amount of hydroxides did not lead to a higher NO_x storage capacity, indicating a negligible role of hydroxides in NO_x storage.

As Raman spectra reveal information not only about the ceria surface structure but also about the bulk, our results allow us to conclude that during NO_x storage not only the surface but also the bulk is involved. The NO_x storage in ceria leads to a redshift of the F_{2g} feature due to the lattice expansion caused by oxygen vacancies in the bulk. As demonstrated by the time-dependent Raman spectra, the redshift was dependent on the consumption of Ce-O sites. As long as Ce-O sites were consumed, a proceeding redshift of the F_{2g} feature was observed, which however stopped as soon as the amount of Ce-O sites

increased. Therefore, the consumption of surface oxygen results in a diffusion of ionic oxygen from the bulk to the surface. Thus, our experiments elucidated a correlation between NO_x storage capacity, Ce-O site consumption, and redshift of the F_{2g} feature.

In the case of NO exposure on oxidized ceria a new reaction pathway was observed, describing the activation of gas-phase oxygen at 30 °C for ionic nitrite transformation. Since the NO_x storage capacity decreased significantly in the absence of gas-phase oxygen and no ionic nitrite transformation was observed anymore, oxygen must have a key role in NO storage, indicating an activation of oxygen on the ceria surface. Since no correlation was found between the peroxides and amount of nitrate and nitrite species formed, the activated oxygen species was not a peroxide. Consequently, upon NO_x storage peroxides are proposed to be only spectators and oxygen is activated differently, leading to an ionic nitrite transformation and re-oxidation of the ceria surface. However, the oxygen activation was not observed at the beginning and is probably dependent on the state of the ceria surface.

Analysis of the NO_x desorption behavior reflects the amount of nitrites ad nitrates formed during NO_x storage. For NO_2 storage and NO/NO_2 storage after oxidative treatment the majority of NO_x was stored as nitrates dominantly desorbing within 200-400°C (62-67%). In contrast, NO/NO_2 storage after reductive treatment mainly lead to preferential formation of nitrites desorbing at temperatures below 200°C (60%). Thus for the ceria material studied the desired PNA property to desorb NO_x within 200-400°C would be best fulfilled for NO_2 storage and NO/NO_2 storage into oxidatively treated ceria.

Acknowledgements

This work was supported by the Deutsche Forschungsgemeinschaft (DFG). Kathrin Hofmann and Silvio Heinschke are acknowledged for XRD and nitrogen adsorption/desorption experiments. The authors thank Pablo Beato (Haldor Topsøe) for support with the fluidized bed implementation and David Krüger for help with some of the Raman experiments.

Appendix A. Supplementary data

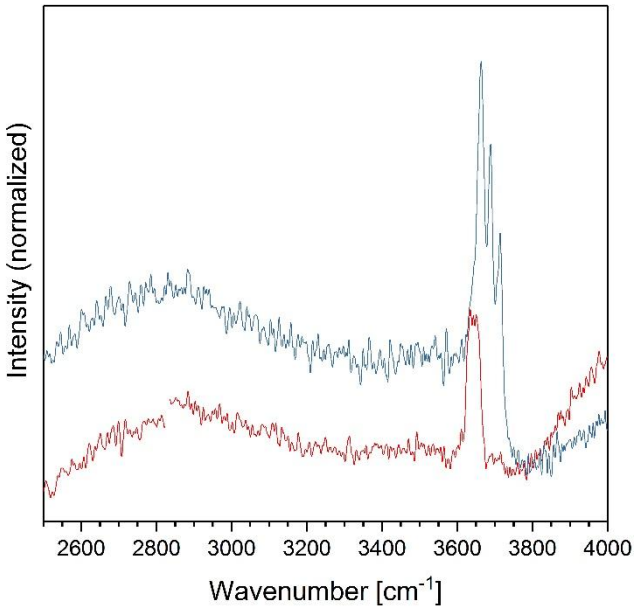

Fig. S1. Enlarged view of Raman spectra of ceria shown in Fig. 2 , recorded at 30°C after oxidative (red) and reductive (blue) pretreatment.

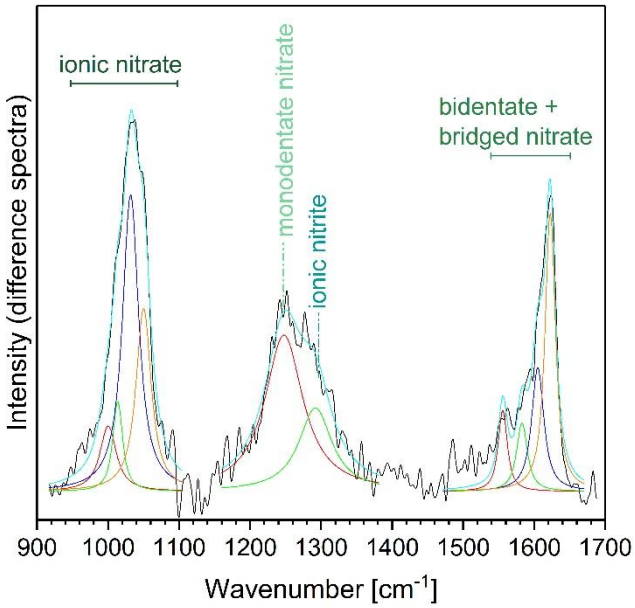

Fig. S2. Least-squares fit analysis of the ionic nitrate, monodentate nitrate, ionic nitrite, and bidentate/bridged nitrate species using Voigt profiles. Difference spectra were obtained by subtracting the normalized spectra of the pretreated ceria from the normalized Raman spectra obtained during NO_x exposure.

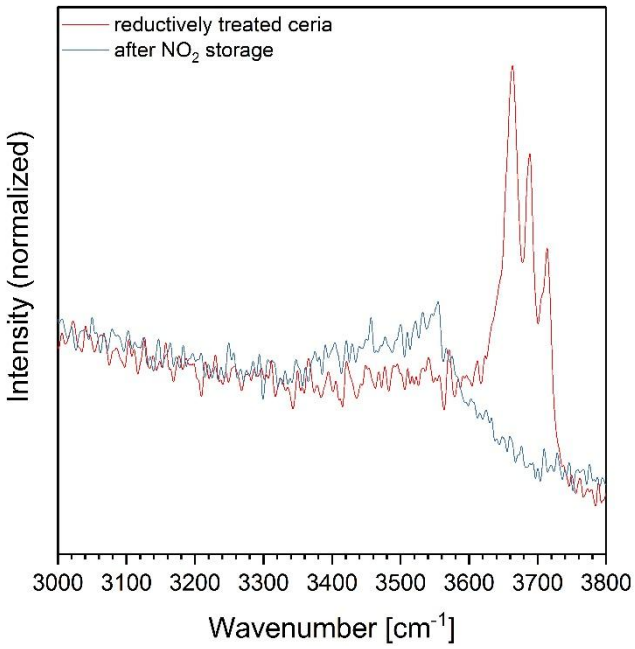

Fig. S3. Raman spectrum of oxidatively treated ceria after 1 h of NO_2 exposure at 30°C showing the range between 3000 and 3800 cm^{-1}.

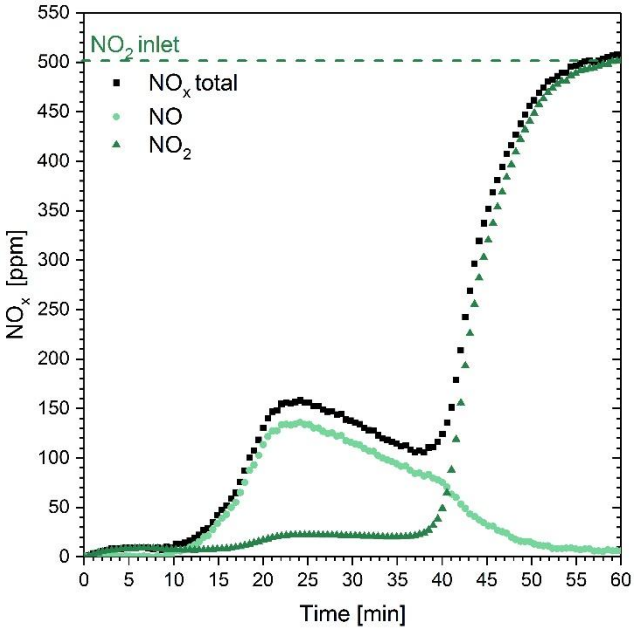

Fig. S4. NO and NO_2 outlet concentrations upon NO_2 exposure on 70 mg of oxidatively treated ceria at 30°C.

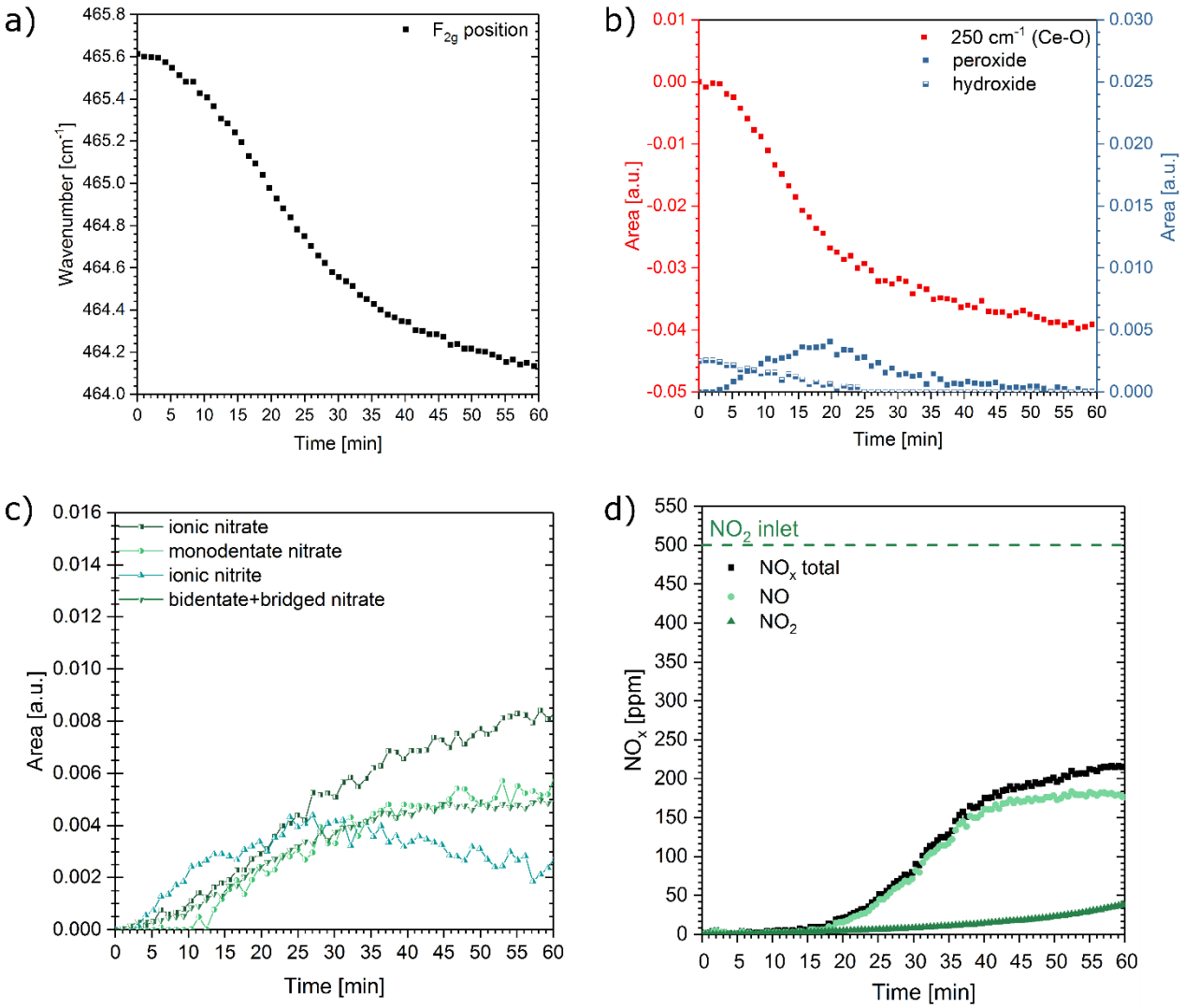

Fig. S5. Temporal evolution of (a) F_{2g} position, (b) Ce-O, peroxide, and hydroxide intensities, and (c) nitrite and nitrate intensities of oxidatively treated ceria upon NO_2 exposure without oxygen at 30°C. Figure S5d depicts the outlet concentrations of NO and NO_2 obtained by FT-IR gas phase analysis, whereas the dashed line shows the NO_2 inlet concentration.

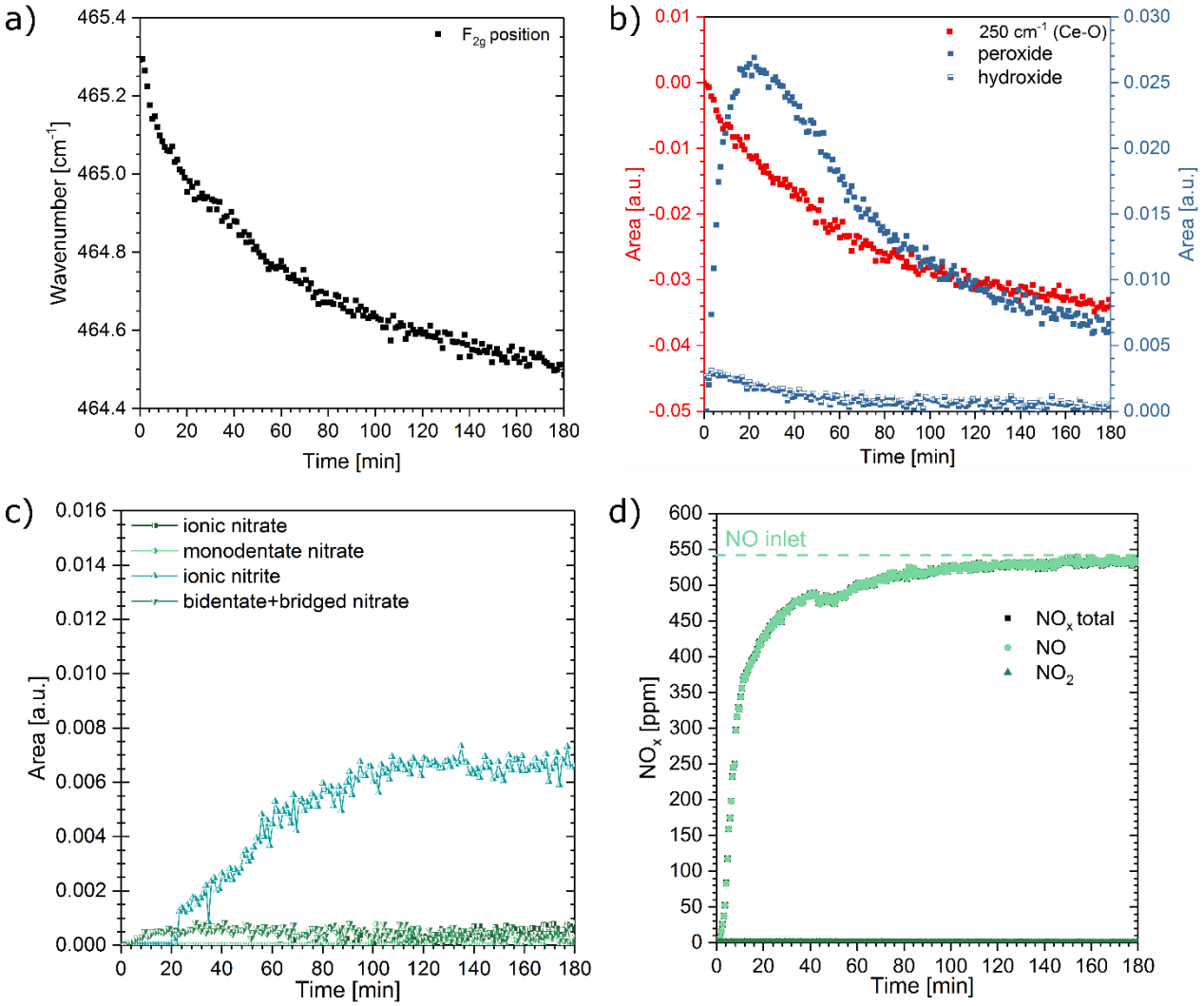

Fig. S6. Temporal evolution of (a) F_{2g} position, (b) Ce-O, peroxide, and hydroxide intensities, and (c) nitrite and nitrate intensities of oxidatively treated ceria upon NO exposure without oxygen at 30°C. Fig. S6d depicts the outlet concentrations of NO and NO_2 obtained by FT-IR gas phase analysis, while the dashed line shows the NO inlet concentration.

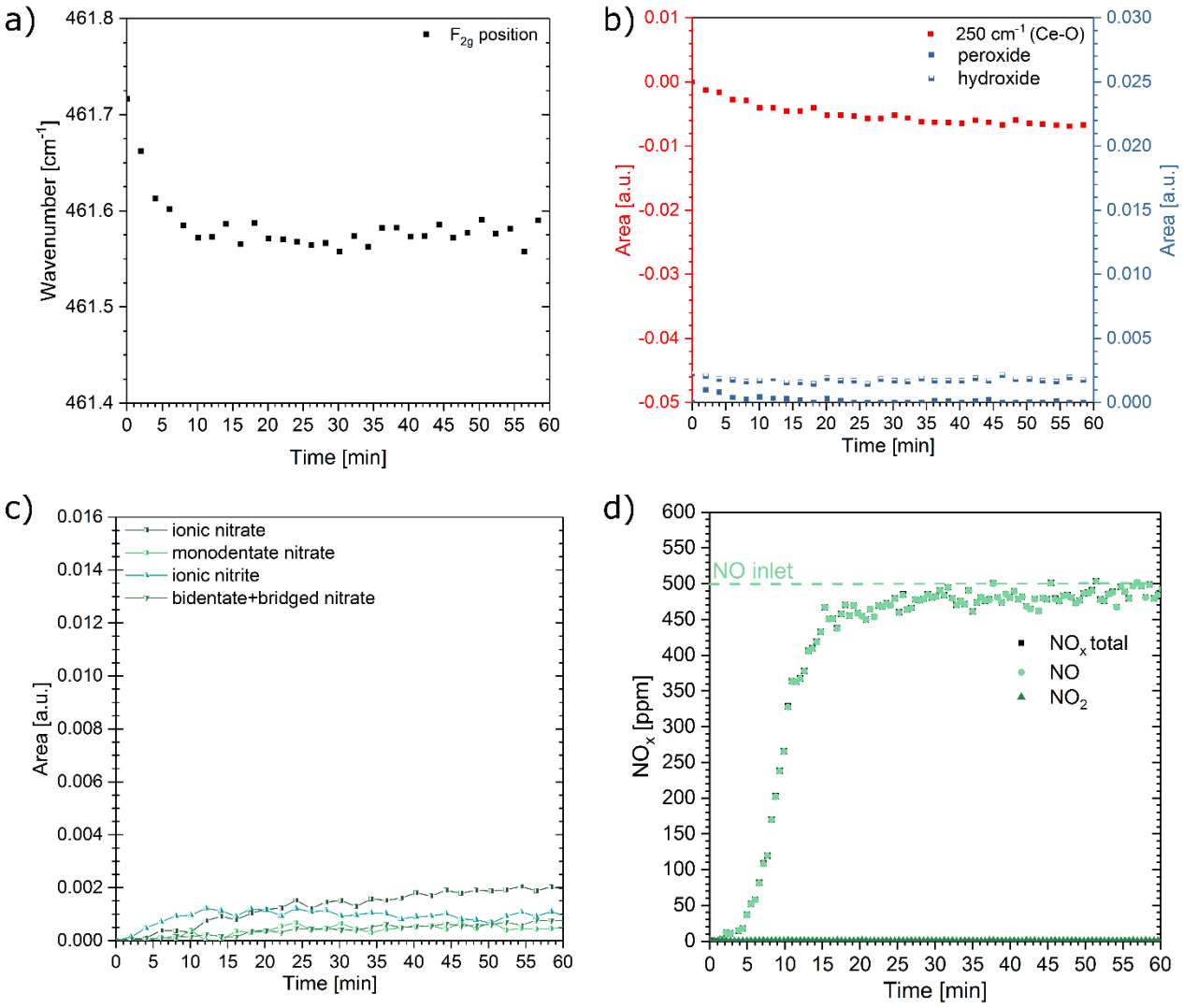

Fig. S7. Temporal evolution of (a) F_{2g} position, (b) Ce-O, peroxide, and hydroxide intensities, and (c) nitrite and nitrate intensities of oxidatively treated ceria upon NO exposure without oxygen at 200°C. Fig. S7d depicts the outlet concentrations of NO and NO_2 obtained by FT-IR gas phase analysis, while the dashed line shows the NO inlet concentration.

References

[1] T.V. Johnson, Review of Vehicular Emissions Trends, SAE Int. J. Engines, 8 (2015) 1152-1166.

[2] G. Guo, D. Dobson, J. Warner, W. Ruona, C.K. Lambert, Advanced Urea SCR System Study with a Ligh Duty Diesel Vehicle, SAE International, (2012) 2012-2001-0371.

[3] J.R. Theis, C.K. Lambert, An assessment of low temperature NO_x adsorbers for cold-start NO_x control on diesel engines, Catal. Today, 258 (2015) 367-377.

[4] J. Wang, Y.Y. Ji, G. Jacobs, S. Jones, D.J. Kim, M. Crocker, Effect of aging on NO_x reduction in coupled LNT-SCR systems, Appl. Catal., B, 148 (2014) 51-61.

[5] J.R. Theis, An assessment of Pt and Pd model catalysts for low temperature NO_x adsorption, Catal. Today, 267 (2016) 93-109.

[6] S.C. Sluder, J.M.E. Storey, S.A. Lewis, L.A. Lewis, Low Temperature Urea Decomposition and SCR Performance, SAE International, 2005.

[7] M. Jarvis, K.M. Adams, Method for converting exhaust gases from a diesel engine using nitrogen oxide absorbent U.S. Patent 6,182,443, 2001.

[8] T.J. Toops, D.B. Smith, W.P. Partridge, NO_x adsorption on $Pt/K/Al_2O_3$, Catal. Today, 114 (2006) 112-124.

[9] T.J. Toops, D.B. Smith, W.P. Partridge, Quantification of the *in situ* DRIFT spectra of $Pt/K/\gamma\text{-}Al_2O_3$ NO_x adsorber catalysts, Appl. Catal., B, 58 (2005) 245-254.

[10] S.S. Chaugule, V.F. Kispersky, J.L. Ratts, A. Yezerets, N.W. Currier, F.H. Ribeiro, W.N. Delgass, Formation and removal of Ba-carbonates or carboxylates on $Pt/BaO/\gamma\text{-}Al_2O_3$ lean NO_x traps, Appl. Catal., B, 107 (2011) 26-33.

[11] C.A. Shi, Y.Y. Ji, U.M. Graham, G. Jacobs, M. Crocker, Z.S. Zhang, Y. Wang, T.J. Toops, NO_x storage and reduction properties of model ceria-based lean NO_x trap catalysts, Appl. Catal., B, 119 (2012) 183-196.

[12] J.H. Kwak, D.H. Kim, T. Szailer, C.H.F. Peden, J. Szanyi, NO_x uptake mechanism on $Pt/BaO/Al_2O_3$ catalysts, Catal. Lett., 111 (2006) 119-126.

[13] Y.Y. Ji, S.L. Bai, M. Crocker, Al_2O_3-based passive NO_x adsorbers for low temperature applications, Appl. Catal., B, 170 (2015) 283-292.

[14] S. Jones, Y.Y. Ji, M. Crocker, Ceria-Based Catalysts for Low Temperature NO_x Storage and Release, Catal. Lett., 146 (2016) 909-917.

[15] Y.Y. Ji, T.J. Toops, U.M. Graham, G. Jacobs, M. Crocker, A kinetic and DRIFTS study of supported Pt catalysts for NO oxidation, Catal. Lett., 110 (2006) 29-37.

[16] J.Y. Luo, W.S. Epling, G.S. Qi, W. Li, Low Temperature Ceria-Based Lean NO_x Traps, Catal. Lett., 142 (2012) 946-958.

[17] Y.Y. Ji, T.J. Toops, J.A. Pihl, M. Crocker, NO_x storage and reduction in model lean NO_x trap catalysts studied by *in situ* DRIFTS, Appl. Catal., B, 91 (2009) 329-338.

[18] L.F. Lv, X.Q. Wang, M.Q. Shen, Q.Q. Zhang, J. Wang, The lean NO_x traps behavior of (1-5 %) BaO/CeO_2 mixed with Pt/Al_2O_3 at low temperature (100-300 °C): The effect of barium dispersion, Chem. Eng. J., 222 (2013) 401-410.

[19] X.Q. Wang, L.F. Lv, Q.Q. Zhang, Y.W. Zhang, J. Wang, M.Q. Shen, The different NO_x trap performance on ceria and barium/ceria containing LNT catalysts below 200 °C, Catal. Sci. Technol., 3 (2013) 200-207.

[20] L. Wang, R. Ran, X.D. Wu, M. Li, D. Weng, In situ DRIFTS study of NO_x adsorption behavior on Ba/CeO_2 catalysts, J. Rare Earth, 31 (2013) 1074-1080.

[21] J.H. Kwak, D.H. Kim, J. Szanyi, C.H.F. Peden, Excellent sulfur resistance of $Pt/BaO/CeO_2$ lean NO_x trap catalysts, Appl. Catal., B, 84 (2008) 545-551.

[22] Y.Y. Ji, D.Y. Xu, S.L. Bai, U. Graham, M. Crocker, B.B. Chen, C. Shi, D. Harris, D. Scapens, J. Darab, Pt- and Pd-Promoted CeO_2-ZrO_2 for Passive NO_x Adsorber Applications, Ind. Eng. Chem. Res., 56 (2017) 111-125.

[23] A. Filtschew, D. Stranz, C. Hess, Mechanism of NO_2 storage in ceria studied using combined *in situ* Raman/FT-IR spectroscopy, Phys. Chem. Chem. Phys., 15 (2013) 9066-9069.

[24] Z. Say, E.I. Vovk, V.I. Bukhtiyarov, E. Ozensoy, Enhanced Sulfur Tolerance of Ceria-Promoted NO_x Storage Reduction (NSR) Catalysts: Sulfur Uptake, Thermal Regeneration and Reduction with H_2(g), Top. Catal., 56 (2013) 950-957.

[25] L. Kylhammar, P.A. Carlsson, H.H. Ingelsten, H. Gronbeck, M. Skoglundh, Regenerable ceria-based SO_x traps for sulfur removal in lean exhausts, Appl. Catal., B, 84 (2008) 268-276.

[26] B. Levasseur, A.M. Ebrahim, T.J. Bandosz, Role of Zr^{4+} Cations in NO_2 Adsorption on $Ce_{1-x}Zr_xO_2$ Mixed Oxides at Ambient Conditions, Langmuir, 27 (2011) 9379-9386.

[27] I. Atribak, B. Azambre, A.B. Lopez, A. Garcia-Garcia, Effect of NO_x adsorption/desorption over ceria-zirconia catalysts on the catalytic combustion of model soot, Appl. Catal., B, 92 (2009) 126-137.

[28] A. Martinez-Arias, J. Soria, J.C. Conesa, X.L. Seoane, A. Arcoya, R. Cataluna, NO reaction at surface oxygen vacancies generated in cerium oxide, J. Chem. Soc., Faraday Trans., 91 (1995) 1679-1687.

[29] M. Nolan, S.C. Parker, G.W. Watson, Reduction of NO_2 on ceria surfaces, J. Phys. Chem. B, 110 (2006) 2256-2262.

[30] M.Y. Mihaylov, E.Z. Ivanova, H.A. Aleksandrov, P. St Petkov, G.N. Vayssilov, K.I. Hadjiivanov, FTIR and density functional study of NO interaction with reduced ceria: Identification of N-3(-) and NO2- as new intermediates in NO conversion, Appl. Catal., B, 176 (2015) 107-119.

[31] B. Azambre, L. Zenboury, A. Koch, J.V. Weber, Adsorption and Desorption of NOx on Commercial Ceria-Zirconia (CexZr1-xO2) Mixed Oxides: A Combined TGA, TPD-MS, and DRIFTS study, J. Phys. Chem. C, 113 (2009) 13287-13299.

[32] N. Maeda, A. Urakawa, A. Baiker, Support Effects and Chemical Gradients along the Catalyst Bed in NO_x Storage-Reduction Studied by Space- and Time-Resolved *In Situ* DRIFTS, J. Phys. Chem. C, 113 (2009) 16724-16735.

[33] M.O. Symalla, A. Drochner, H. Vogel, S. Philipp, U. Gobel, W. Muller, IR-study of formation of nitrite and nitrate during NO_x-adsorption on NSR-catalysts-compounds CeO_2 and BaO/CeO_2, Top. Catal., 42-43 (2007) 199-202.

[34] A. Urakawa, N. Maeda, A. Baiker, Space- and Time-Resolved Combined DRIFT and Raman Spectroscopy: Monitoring Dynamic Surface and Bulk Processes during NO_x Storage Reduction, Angew. Chem., Int. Ed., 47 (2008) 9256-9259.

[35] S. Philipp, A. Drochner, J. Kunert, H. Vogel, J. Theis, E.S. Lox, Investigation of NO adsorption and NO/O-2 co-adsorption on NOx-storage-components by DRIFT-spectroscopy, Top. Catal., 30-1 (2004) 235-238.

[36] J.A. Rodriguez, T. Jirsak, S. Sambasivan, D. Fischer, A. Maiti, Chemistry of NO2 on CeO2 and MgO: Experimental and theoretical studies on the formation of NO3, J Chem Phys, 112 (2000) 9929-9939.

[37] G. Liu, J.A. Rodriguez, J. Hrbek, J. Dvorak, C.H.F. Peden, Electronic and chemical properties of Ce0.8Zr0.2O2(111) surfaces: Photoemission, XANES, density-functional, and NO2 adsorption studies, J. Phys. Chem. B, 105 (2001) 7762-7770.

[38] A. Filtschew, K. Hofmann, C. Hess, Ceria and Its Defect Structure: New Insights from a Combined Spectroscopic Approach, J. Phys. Chem. C, 120 (2016) 6694-6703.

[39] C. Schilling, A. Hofmann, C. Hess, M.V. Ganduglia-Pirovano, Raman Spectra of Polycrystalline CeO_2: A Density Functional Theory Study, J. Phys. Chem. C, 121 (2017) 20834-20849.

[40] P. Beato, E. Schachtl, K. Barbera, F. Bonino, S. Bordiga, Operando Raman spectroscopy applying novel fluidized bed micro-reactor technology, Catal. Today, 205 (2013) 128-133.

[41] B. Azambre, L. Zenboury, J.V. Weber, P. Burg, Surface characterization of acidic ceria-zirconia prepared by direct sulfation, Appl Surf Sci, 256 (2010) 4570-4581.

[42] J.R. Mcbride, K.C. Hass, B.D. Poindexter, W.H. Weber, Raman and X-Ray Studies of $Ce_{1-x}Re_xO_{2-Y}$, Where Re=La, Pr, Nd, Eu, Gd, and Tb, J. Appl. Phys., 76 (1994) 2435-2441.

[43] W.H. Weber, K.C. Hass, J.R. Mcbride, Raman-Study of CeO_2 - 2nd-Order Scattering, Lattice-Dynamics, and Particle-Size Effects, Phys. Rev. B, 48 (1993) 178-185.

[44] V.V. Pushkarev, V.I. Kovalchuk, J.L. d'Itri, Probing Defect Sites on the CeO_2 Surface with Dioxygen, J. Phys. Chem. B, 108 (2004) 5341-5348.

[45] Y.M. Choi, H. Abernathy, H.T. Chen, M.C. Lin, M.L. Liu, Characterization of O_2-CeO_2 interactions using *in situ* Raman spectroscopy and first-principle calculations, ChemPhysChem, 7 (2006) 1957-1963.

[46] C. Binet, A. Badri, J.C. Lavalley, A Spectroscopic Characterization of the Reduction of Ceria from Electronic-Transitions of Intrinsic Point-Defects, J. Phys. Chem., 98 (1994) 6392-6398.

[47] A. Badri, C. Binet, J.C. Lavalley, An FTIR study of surface ceria hydroxy groups during a redox process with H_2, J. Chem. Soc., Faraday Trans., 92 (1996) 4669-4673.

[48] A. Filtschew, C. Hess, Interpretation of Raman Spectra of Oxide Materials: The Relevance of Absorption Effects, J. Phys. Chem. C, 121 (2017) 19280-19287.

[49] N. Sergent, M. Epifani, T. Pagnier, In situ Raman spectroscopy study of NO_2 adsorption onto nanocrystalline tin(IV) oxide, J. Raman Spectrosc., 37 (2006) 1272-1277.

[50] C. Hess, J.H. Lunsford, Mechanism for NO_2 storage in barium oxide supported on magnesium oxide studied by *in situ* Raman spectroscopy, J. Phys. Chem. B, 106 (2002) 6358-6360.

[51] K.I. Hadjiivanov, Identification of neutral and charged N_xO_y surface species by IR spectroscopy, Catal. Rev. - Sci. Eng., 42 (2000) 71-144.

[52] I.A. Degen, G.A. Newman, Raman-Spectra of Inorganic-Ions, Spectrochim. Acta, Part A, 49 (1993) 859-887.

[53] M. Molinari, S.C. Parker, D.C. Sayle, M.S. Islam, Water Adsorption and Its Effect on the Stability of Low Index Stoichiometric and Reduced Surfaces of Ceria, J. Phys. Chem. C, 116 (2012) 7073-7082.

[54] C. Descorme, Y. Madier, D. Duprez, Infrared study of oxygen adsorption and activation on cerium-zirconium mixed oxides, J. Catal., 196 (2000) 167-173.

[55] C. Schilling, C. Hess, Real-Time Observation of the Defect Dynamics in Working Au/CeO_2 Catalysts by Combined Operando Raman/UV-Vis Spectroscopy, J. Phys. Chem. C, 122 (2018) 2909-2917.

[56] L. Zhang, J. Pierce, V.L. Leung, D. Wang, W.S. Epling, Characterization of Ceria's Interaction with NOx and NH3, J. Phys. Chem. C, 117 (2013) 8282-8289.

[57] Please note that the activated oxygen species proposed to be formed according to eq. 20 corresponds to the one given in eq. 5 from the literature.

*Graphical Abstract

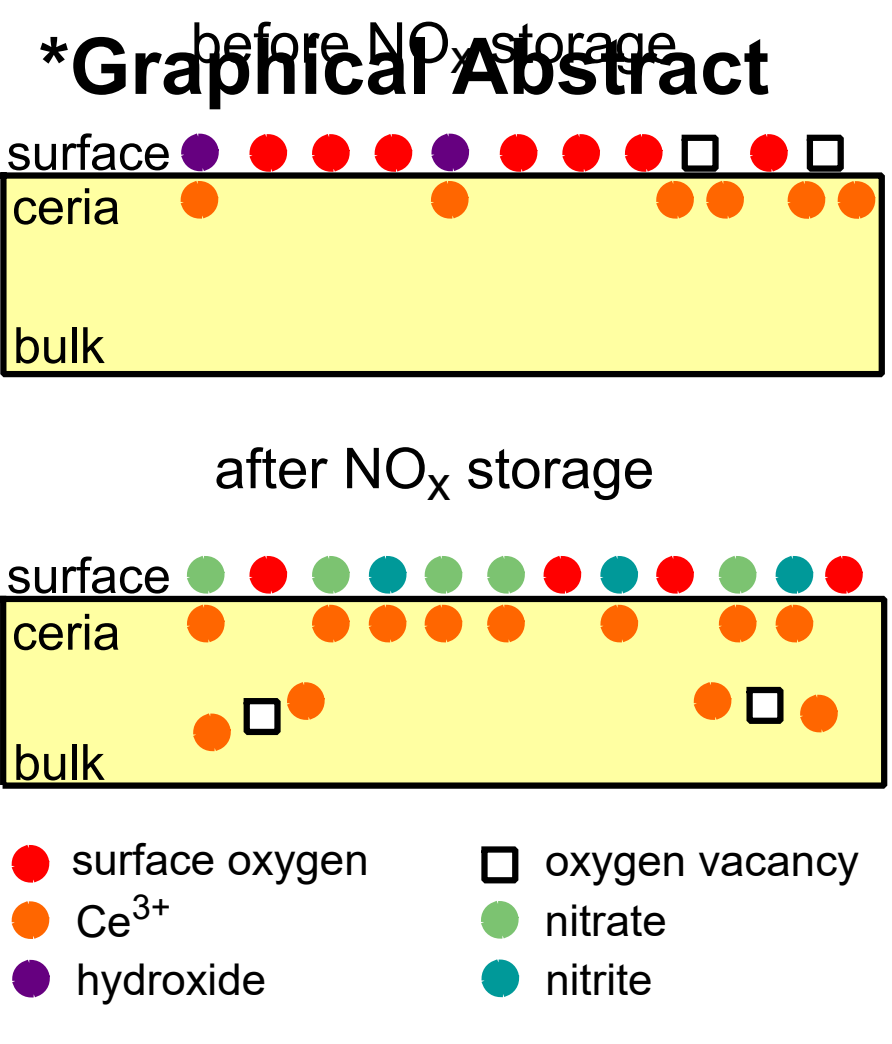

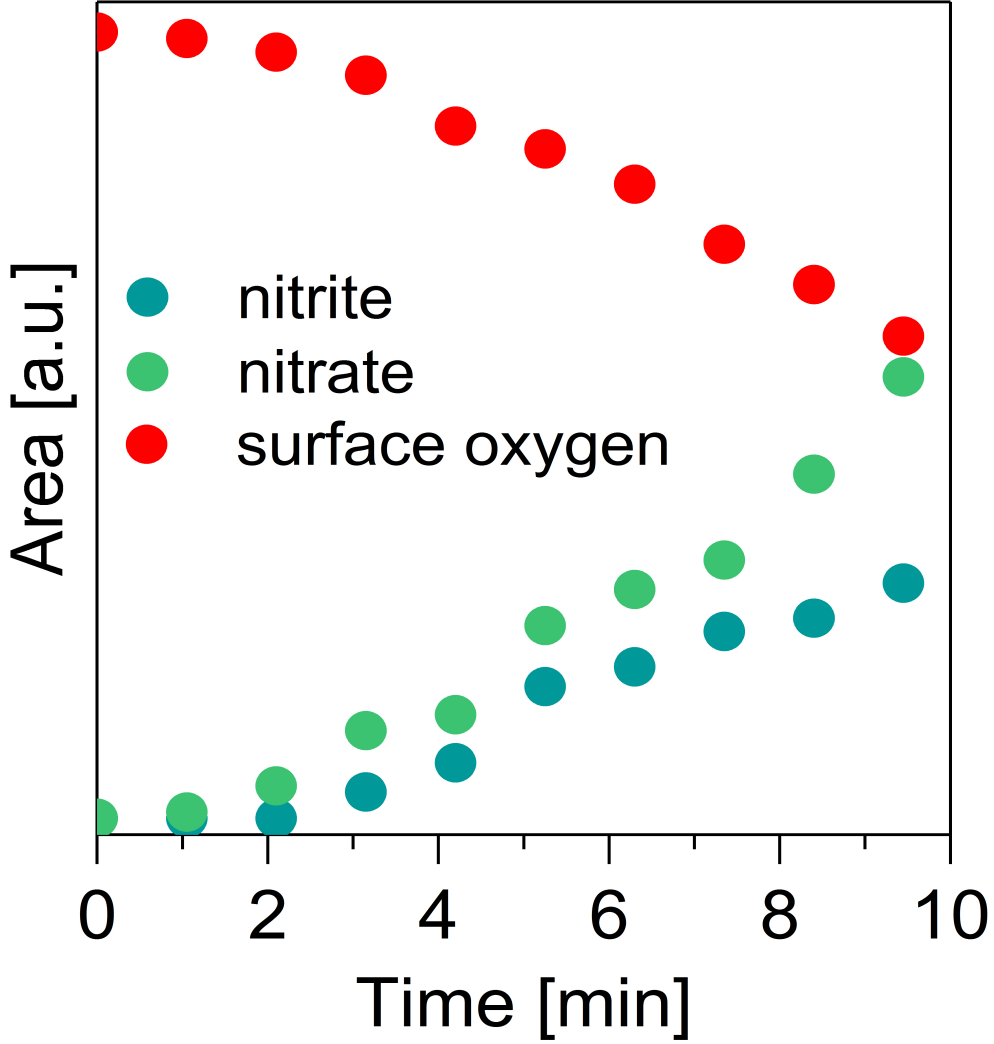

***Highlights (for review)**

- Dynamics of ceria surface and bulk structure during NO_x storage monitored.
- Spectroscopic evidence for Ce-O involvement in NO_x storage.
- New reaction pathways postulated for activation of gas-phase oxygen.
- New insight into mechanisms for NO and NO_2 storage in ceria.